TXNIP mediates LAT1/SLC7A5 endocytosis to reduce amino acid uptake in cells entering quiescence

Jennifer Kahlhofer[1,2], Nikolas Marchet[1,2], Brigitta Seifert[2], Kristian Zubak[1], Madlen Hotze[3], Anna-Sophia Egger[3], Claudia Manzl[4], Yannick Weyer[1,2], Sabine Weys[2,5], Martin Offterdinger[6], Sebastian Herzog[7], Veronika Reiterer[8], Marcel Kwiatkowski[3], Saskia B. Wortmann[9,10], Siamak Nemati[11], Johannes A. Mayr[9], Johannes Zschocke[12], Bernhard Radlinger[13], Kathrin Thedieck[3,15], Lukas A. Huber[2], Hesso Farhan[8], Mariana E.G. de Araujo[2], Susanne Kaser[13], Sabine Scholl-Bürgi[14], Daniela Karall[14], and David Teis[1,2+]

[1] Institute of Molecular Biochemistry, Biocenter, Medical University of Innsbruck, 6020 Innsbruck, Austria.
[2] Institute of Cell Biology, Biocenter, Medical University of Innsbruck, 6020 Innsbruck, Austria.
[3] Department of Biochemistry and Center for Molecular Biosciences Innsbruck, University of Innsbruck, 6020 Innsbruck, Austria
[4] Institute of Pathology, Neuropathology & Molecular Pathology, Medical University of Innsbruck, 6020 Innsbruck, Austria.
[5] Institute of Science and Technology Austria (ISTA), 3400 Klosterneuburg, Austria.
[6] Institute of Neurobiochemistry, BioOptics core facility, Biocenter, Medical University of Innsbruck, 6020 Innsbruck, Austria.
[7] Institute for Developmental Immunology, Biocenter, Medical University of Innsbruck, 6020 Innsbruck, Austria.
[8] Institute of Pathophysiology, Biocenter, Medical University of Innsbruck, 6020 Innsbruck, Austria.
[9] University Children's Hospital, Salzburger Landeskliniken and Paracelsus Medical University, 5020 Salzburg, Austria.
[10] Amalia Children's Hospital, Department of Pediatrics, Pediatric Neurology, Nijmegen, The Netherlands
[11] Kinder- und Jugendheilkunde, Krankenhaus St. Vinzenz Zams, 6511 Zams, Austria
[12] Institute of Human Genetics, Medical University of Innsbruck, 6020 Innsbruck, Austria.
[13] Department of Internal Medicine I, Medical University of Innsbruck, 6020 Innsbruck, Austria.
[14] Department of Child and Adolescent Health, Division of Pediatrics I-Inherited Metabolic Disorders, Medical University of Innsbruck, 6020 Innsbruck, Austria.
[15] Department Metabolism, Senescence and Autophagy, Research Center One Health Ruhr, University Alliance Ruhr & University Hospital Essen, University Duisburg-Essen, Essen; German Cancer Consortium (DKTK), partner site Essen, a partnership between German Cancer Research Center (DKFZ) and University Hospital Essen, Heidelberg; Freiburg Materials Research Center (FMF), University Freiburg, Freiburg, Germany; Laboratory of Pediatrics, Section Systems Medicine of Metabolism and Signaling, University of Groningen, University Medical Center Groningen, Groningen, Netherlands.

[+]corresponding author:
David Teis, PhD
Institute for Molecular Biochemistry, Medical University of Innsbruck
Innrain 80/82, CCB Building
A-6020, Innsbruck, Austria
tel: +43512900370191
email: david.teis@i-med.ac.at

Abstract

Entry and exit from cellular quiescence require dynamic adjustments in nutrient acquisition, yet the mechanisms by which quiescent cells downregulate amino acid (AA) transport remain poorly understood. Here, we demonstrate that cells entering quiescence select plasma membrane-resident AA transporters for endocytosis and lysosomal degradation, to match AA uptake with reduced translation. We identify the α-arrestin TXNIP as a key regulator of AA uptake during quiescence, since it mediates the endocytosis of the SLC7A5-SLC3A2 (LAT1-4F2hc) transporter complex in response to reduced AKT signaling. Mechanistically, TXNIP interacts with HECT-type ubiquitin ligases to facilitate transporter ubiquitination. Loss of TXNIP disrupts this regulation, resulting in dysregulated AA uptake, sustained mTORC1 signaling, and accelerated quiescence exit. A novel TXNIP loss-of-function mutation in a patient with severe metabolic disease further supports its role in nutrient homeostasis and human health. These findings highlight TXNIP's role in controlling SLC7A5-SLC3A2 mediated AA acquisition with implications for quiescence biology and disease.

Introduction

How cells maintain a homeostatic pool of 20 proteinogenic amino acids (AA) is a fundamental question in biology. For the uptake and the release of AA across the plasma membrane (PM) and across organelle membranes, the human genome encodes at least 66 AA transporters, which belong to 11 individual solute carrier (SLC) families [1,2]. The importance of controlling AA transport is exemplified by monogenic diseases and human pathologies caused by the deficiency or dysregulation of individual AA transporters [3,4].

Cellular AA import is coordinated with cell proliferation. Proliferating cells, in particular cancer cells, increase the abundance of AA transporters at the cell surface and thereby promote nutrient uptake for protein synthesis during cell growth prior to cell division [5]. Transcriptional mechanisms are responsible for the upregulation of AA transporter expression [6-9].

Conversely, entry into quiescence, the reversible exit from the cell cycle, is accompanied by a reduction in cell size, lower rates of transcription, and reduced protein synthesis [10,11]. Thus, quiescent cells must somehow re-calibrate AA uptake to align it with lower translation and metabolic homeostasis for cell survival, rather than for growth [12]. How quiescent cells match AA flux across the PM to reduced cell size and to lower translation rates is unclear. This presents a knowledge gap in understanding cellular nutrient acquisition.

In budding yeast, *Saccharomyces cerevisiae*, we previously demonstrated that entry into quiescence induces the ubiquitin dependent endocytosis of AA transporters [13]. The selective ubiquitination of AA transporters requires proteins of the α-arrestin family [14 15]. Activated α-arrestins function as adaptor proteins that recruit the homologous to the E6-AP carboxyl terminus (HECT) type ubiquitin ligase Rsp5 to different AA transporters for ubiquitination, endocytosis and lysosomal degradation [16-18].

The human genome encodes six α-arrestin family members or ARRDCs (arrestin-domain-containing proteins). With the exception of ARRDC5, α-arrestins contain one or more PPxY motifs in their C-terminal regions and are able to interact with several HECT-type ubiquitin ligases [19-22]. The best characterized α-arrestin is thioredoxin interacting protein (TXNIP). TXNIP was first described as a negative regulator of thioredoxin (TRX) through the formation of an intermolecular disulfide bond that requires two critical cysteine residues of TXNIP (cysteine 32 and cysteine 247) [23-25].

TXNIP also regulates glucose uptake by mediating the selective endocytosis of SLC2A1 (GLUT1) and SLC2A4 (GLUT4), two major glucose transporters. TXNIP binds to these glucose transporters at the PM and interacts with a di-leucine motif in its C-terminal tail with components of the endocytic machinery [26,27]. The TXNIP dependent regulation of SLC2A1 and

99 SLC2A4 is tightly coupled to intracellular glucose homeostasis, ATP availability and growth
100 factor signaling. AMPK activation in response to low ATP levels or AKT activation in response
101 to insulin signal results in the phosphorylation of TXNIP at serine 308, thereby inactivating it
102 [26,27]. This inactivation of TXNIP ensures SLC2A1 and SLC2A4 accumulation at the PM to
103 increase glucose uptake [26,27]. TXNIP inactivation can involve ubiquitination by the HECT-type
104 ubiquitin ligase ITCH, leading to its proteasomal degradation [19,22]. These processes appear to
105 be largely independent of TRX binding. Consistent with the function in regulating glucose
106 uptake, biallelic loss-of-function mutations in TXNIP in humans lead to lactic acidosis in three
107 siblings. Interesting, these patients also showed lower serum methionine levels [28].
108 Here, we show that in human cells entering quiescence, several AA transporters are selectively
109 removed from the PM by endocytosis, including the heterodimeric AA transporter (HAT)
110 SLC7A5-SLC3A2 (LAT1-4F2hc). The endocytic degradation of SLC7A5-SLC3A2 during
111 entry into quiescence requires TXNIP. TXNIP uses its PPxY motifs to engage HECT-type
112 ubiquitin ligases for SLC7A5-SLC3A2 endocytosis and subsequent lysosomal degradation.
113 The TXNIP mediated endocytic degradation of SLC7A5-SLC3A2 reduces AA uptake, lowers
114 free intracellular AA levels, and thereby helps to dampen mTORC1 signaling and translation.
115 In growing cells, AKT phosphorylation of TXNIP restricts SLC7A5-SLC3A2 endocytosis. In
116 addition, we identified a novel biallelic loss-of-function TXNIP variant in a boy with a severe
117 inborn metabolic disease. The analysis of fibroblasts from this patient revealed that SLC7A5-
118 SLC3A2 endocytosis was also blocked. This further supports the central role of TXNIP in
119 adjusting cellular AA uptake, with important implications for human health.
120
121 **Results**
122
123 **Selective endocytosis and lysosomal degradation of AA transporters in cells entering**
124 **quiescence.**
125 To study the regulation of nutrient uptake during the transition from proliferation to quiescence,
126 we used hTERT RPE1 cells (non-cancerous human telomerase-immortalized retinal pigmented
127 epithelial, hereafter RPE1) as a model cell line [29,30]. First, we established and evaluated
128 conditions for entry into quiescence.
129 The DNA content of cells growing with serum was analyzed by propidium iodide (PI) staining
130 and fluorescence activated cell sorting (FACS). 46% (± 2%) of these cells were in the G0/G1
131 phase of the cell cycle, 30% (± 6%) were in S phase and 24% (± 4%) in the G2/M phase. 24 h
132 after serum starvation (but in the presence of AA and glucose), the number of cells in G0/G1
133 increased to 67% (± 10%), while the number of cells in S-phase and G2/M phase decreased to

134 15% (± 6%) and 19% (± 7%), respectively (Figure 1a). Cell viability was not affected by serum
135 starvation (Supplementary Figure 1a). Serum starved cells also decreased their volume by 20%
136 from 2907 fl to 2332 fl (Figure 1b). Consistent with an entry into quiescence in response to
137 serum starvation, SDS-PAGE and Western Blot (WB) analysis of total cell lysates showed that
138 the protein levels of the cyclin-dependent kinase inhibitor $p27^{Kip1}$ increased, while the
139 phosphorylation dependent activation of mitogen activated kinases ERK1/2, and mTORC2-
140 dependent phosphorylation of AKT on serine 473 decreased (Figure 1c, lane 2).
141 Of note, in cells entering quiescence, the protein levels of the heterodimeric AA transporters
142 (HAT) SLC7A5-SLC3A2 (LAT1-4F2hc) and SLC7A11-SLC3A2 (xCT-4F2hc) decreased
143 (Figure 1c, lane 1 and 2). Also, a decrease in the protein levels of SLC1A5 (ASCT2) was
144 detected (Figure 1c, lane 1 and 2). The protein levels of the neutral AA transporter SLC38A2
145 (SNAT2), the glucose transporter SLC2A1 (GLUT1), the transferrin receptor TfR and
146 epidermal growth factor receptor (EGFR) remained relatively unchanged over the course of the
147 experiment (Figure 1c, lane 1 - 3). The downregulation of SLC7A5 and SLC1A5 was observed
148 in other non-cancerous cell lines, such as mouse embryonic fibroblasts (MEFs) (Supplementary
149 Figure 1b) and primary human fibroblasts (Supplementary Figure 1c, d), when subjected to
150 serum starvation. However, this downregulation was not observed in a panel of seven different
151 lung cancer cell lines (Supplementary Figure 1e).
152 To understand how SLC7A5-SLC3A2 and SLC1A5 were downregulated in cells entering
153 quiescence, we examined the localization of these transporters using indirect
154 immunofluorescence (IF) and confocal microscopy. In growing cells, endogenous SLC3A2
155 (Figure 1e) and SLC1A5 (Supplementary Figure 1f) were mainly detected at the PM and
156 partially co-localized with LAMP1 positive lysosomes (Figure 1e and Supplementary Figure
157 1f). In serum starved cells, signals for SLC3A2 were barely detected (Figure 1e), which was in
158 line with the downregulation of SLC7A5-SLC3A2 in quiescent cells. Also, cell surface FACS
159 analysis measured a marked decrease of PM resident SLC3A2 (Figure 1d). Treatment of cells
160 with chloroquine (CQ), which impairs lysosomal catabolic function, resulted in the
161 accumulation of SLC3A2 (Figure 1e) and SLC1A5 (Supplementary Figure 1f) inside LAMP1
162 positive lysosomes and efficiently prevented the lysosomal degradation of these AA
163 transporters (Figure 1f). Inhibition of the GTPase dynamin with dynasore (dyna), which blocks
164 the scissions of clathrin coated vesicles from the PM [31,32], impaired the endocytosis of SLC3A2
165 (Fig 1g) and SLC1A5 (Supplementary Figure 1g) and in consequence prevented their lysosomal
166 degradation (Figure 1h).

167 In line with the quiescence induced endocytic removal of SLC7A5-SLC3A2 from the PM, the
168 uptake of its AA substrates [^{3}H]-leucine and [^{14}C]-isoleucine was reduced by 33% and 49%,
169 respectively (Figure 1i). Similarly, the uptake of the SLC1A5 substrate [^{14}C]-glutamine
170 decreased by 20% (Supplementary Figure 1g).
171 The decrease in AA uptake upon entry into quiescence correlated with a reduction of mTORC1
172 signaling (*e.g.* towards S6K) and with an increase of eIF2α phosphorylation at serine 51 (Figure
173 1c, line 1 and 2), indicating a downregulation of translation. Consistently, the incorporation of
174 [^{35}S]-methionine and [^{35}S]-cysteine into newly synthesized proteins was reduced in quiescent
175 cells (Figure 1j, line 1 and 2).
176 Upon re-addition of serum to starved cells, SLC7A5-SLC3A2, SLC7A11-SLC3A2, and
177 SLC1A5 protein levels were upregulated, ERK-, AKT- as well as mTORC1-signaling were re-
178 activated, phosphorylation of eIF2α decreased as did p27^{Kip1} protein levels (Figure 1c, lane 3).
179 Translation (Figure 1j, lane 3) and cell size increased (Figure 1c), and cells resumed
180 proliferation (Figure 1a).
181 These results showed that the selective endocytosis and degradation of SLC7A5-SLC3A2
182 coincided with a decrease in cell volume, with a drop in translation, and with a reduction in
183 (iso)leucine uptake as cells entered quiescence in response to serum starvation.
184
185 **TXNIP is required for the selective downregulation of SLC7A5**
186 To identify the molecular mechanism responsible for the quiescence induced endocytic
187 degradation of SLC7A5-SLC3A2, we focused on the α-arrestin family of ubiquitin ligase
188 adaptors. α-arrestins are required for the endocytic downregulation of AA transporters in
189 budding yeast cells entering quiescence [13,33]. It was not known if they had a similar function in
190 human cells.
191 The human genome encodes six α-arrestins, called ARRDC (arrestin domain containing) 1-5,
192 and TXNIP [15]. TXNIP protein levels (Figure 2a, b) and mRNA levels (Supplementary Figure
193 2a) increased in response to serum starvation.
194 To determine whether TXNIP contributed to SLC7A5-SLC3A2 endocytosis and lysosomal
195 degradation, we used CRISPR/Cas9 mediated gene editing and introduced a 13 base pair
196 deletion at position c.644_656 leading to a frameshift that resulted in a premature stop codon
197 at position 226 (p.I215TfsTer11) (Supplementary Figure 2b, c). This mutation disrupted the
198 architecture of the arrestin C-domain (Supplementary Figure 2b) and in single cell clones, the
199 mutant protein was no longer detected (Figure 2a).

200 The loss-of-function mutation in TXNIP selectively prevented the endocytic downregulation of
201 the SLC7A5-SLC3A2 heterodimer (Figure 2a, lane 2, and Figure 2b). In TXNIP^{KO} cells,
202 SLC3A2 remained at the PM in response to serum starvation, as determined by IF and cell
203 surface FACS (Figure 2c, d and Supplementary Figure 2d). Re-expression of TXNIP in
204 TXNIP^{KO} cells restored SLC7A5-SLC3A2 endocytosis and degradation in response to serum
205 starvation (Figure 2c, d and Supplementary Figure 2d - f). Conversely, TXNIP was not required
206 for the degradation of SLC7A11 and SLC1A5 (Figure 2a, lane 2 and Supplementary Figure
207 2b). Hence, in cells entering quiescence, TXNIP selectively targeted SLC7A5-SLC3A2 for
208 endocytosis and degradation. Loss of TXNIP did not affect SLC7A5 mRNA levels
209 (Supplementary Figure 2g).
210 To examine the localization of TXNIP, ALFA-tagged TXNIP (ALFA-TXNIP) was re-
211 expressed in TXNIP^{KO} cells. Using confocal microscopy, we detected a fraction of ALFA-
212 tagged TXNIP at the PM, where it partially co-localized with SLC3A2 [27,34] in proliferating
213 cells, and 7 h after serum starvation (Figure 2e). 24 h after serum starvation, the majority of
214 SLC3A2 was endocytosed and also ALFA-TXNIP was no longer detected at the PM (Figure
215 2e). Under all conditions, ALFA-TXNIP also localized prominently to the nucleus and to the
216 cytosol, as previously observed [35] (Figure 2e).
217 TXNIP has been shown to be required for controlling cellular glucose uptake, by regulating
218 clathrin mediated endocytosis of the glucose transporters SLC2A1 and SLC2A4 in response to
219 glucose depletion or insulin signaling [26,27,36,37]. In WT and in TXNIP^{KO} RPE1 cells entering
220 quiescence, SLC2A1 remained at the PM (Supplementary Figure 2h) and the protein levels of
221 SLC2A1 rather increased in response to serum starvation (Supplementary Figure 2i).
222 Consistently, the uptake of the fluorescent glucose analog 2-NBDG (2-[N-(7-nitrobenz-2-oxa-
223 1,3-diazol-4-yl)amino]-2-deoxy-D-glucose) also increased in cell entering quiescence
224 (Supplementary Figure 2j) [38]. In the TXNIP^{KO} cells, 2-NBDG uptake was moderately elevated
225 already in growing cells (Supplementary Figure 2j).
226 Our data suggested that TXNIP was required for the selective endocytic degradation of the
227 heterodimer SLC7A5-SLC3A2 in cells entering quiescence. Since entering into quiescence did
228 not trigger SLC2A1 endocytosis, it seemed that the TXNIP mediated downregulation of
229 SLC7A5-SLC3A2 was not linked to TXNIP mediated SLC2A1 endocytosis.
230
231 **Identification of a novel TXNIP loss-of-function mutation in a patient with an inborn**
232 **metabolic disorder**

233 TXNIP deficiency caused by a loss-of-function variant c.174_175delinsTT has been previously
234 reported in three sibling with congenital lactic acidosis, low serum methionine levels, variable
235 hypoglycaemia and other metabolic alterations [28]. During the course of the study, we identified
236 a novel TXNIP loss-of-function mutation in another patient. The boy was born in 2014 and
237 presented immediately after birth with recurrent hypoglycemia and muscular hypotonia in
238 conjunction with lactic acidosis (Supplementary Table 1). Subsequently, he showed global
239 developmental delay and marked intellectual disability with autistic features. In addition, he
240 developed epileptic seizures with increasing frequencies of up to 3-4 per month (controlled with
241 levetiracetame, topiramate and lamotrigine). With time, blood glucose concentrations stabilized
242 (Supplementary Table 1), but the boy experienced recurrent hypoglycaemia in response to
243 metabolic stress, e.g., infections. There were consistent metabolic alterations compatible with
244 an AA transporter deficiency. Blood plasma concentrations of several large neutral amino acids
245 (LNAAs, including L, I, V) were elevated throughout the years 2014 – 2022 (Supplementary
246 Table 1). The increased molar ratio of the LNAAs (L, I, V) to aromatic AAs (F, Y), resulted in
247 an elevated Fischer's ratio (FR, 2014: FR = 4.46; 2016: FR = 5.38, 2018: FR = 5.90; 2021; FR=
248 6.98; 2022: FR = 4.23; FR reference range = 2.10 - 4). The methionine levels are not
249 dramatically altered (Supplementary Table 1).
250 Whole-exome sequencing from peripheral blood of the patient detected a homozygous single
251 nucleotide insertion c.642_643insT in exon 5 of 8 of the *TXNIP* gene, which was not recorded
252 in the population genetic variant database gnomAD that lists *TXNIP* as likely haplosufficient
253 (pLI = 0, LOEUF = 0,709: https://gnomad.broadinstitute.org accessed Sept. 10, 2024). The
254 variant caused a frameshift and a premature stop codon after 59 AA (denoted
255 p.Ile215TyrfsTer59), likely causing nonsense-mediated decay (NMD) or the synthesis of a
256 severely truncated TXNIP protein (Figure 3a). Both parents are healthy heterozygous carriers
257 for the variant. No other (likely) pathogenic variant was identified as explanation of the clinical
258 features in the child.
259 To examine how the loss-of-function mutation in TXNIP affected SLC7A5 downregulation,
260 we generated primary patient-derived fibroblasts. WB analysis of the patient fibroblasts showed
261 complete loss of the TXNIP protein (Figure 3b). In these cells, SLC7A5 was no longer
262 downregulated in response to serum starvation (Figure 3b). Furthermore, indirect IF and
263 confocal microscopy showed that SLC3A2 remained at the PM in response to serum starvation
264 in the patient-derived fibroblasts with the TXNIP loss-of-function mutation, but not in the
265 control primary fibroblasts (Figure 3c).

266 To directly test if the patient mutation was causative for the failure to downregulate SLC7A5-
267 SLC3A2, we expressed an ALFA-tagged version cDNA encoding TXNIP p.Ile215TyrfsTer59
268 (ALFA-patient^{mut}, or patient^{mut}) in RPE1 TXNIP^{KO} cells, under the control of a constitutive
269 eIF1α promoter. Under these conditions (which do not trigger NMD), the expression of a
270 truncated TXNIP protein was detected (Figure 3d, lane 3 and 4). ALFA-patient^{mut} localized to
271 the PM, but failed to mediate SLC7A5-SLC3A2 endocytosis in response to serum starvation
272 (Figure 3d-f). Hence, even if the protein was expressed, the TXNIP patient^{mut} protein was non-
273 functional.
274 It seemed that a loss-of-function mutation in TXNIP caused a severe metabolic disease,
275 inhibited the downregulation of SLC7A5-SLC3A2 in patient-derived fibroblasts upon entry
276 into quiescence and caused persistent changes in AA levels in the serum of the affected patient.
277
278 **PPxY motifs of TXNIP were required for the endocytosis of SLC7A5**
279 TXNIP contains two PPxY motifs in its C-terminal region (Figure 4a), which enable the
280 interaction with different HECT type ubiquitin ligases that contain a WW domain [15,19-22,39,40].
281 To test how the PPxY motifs of TXNIP contributed to SLC7A5-SLC3A2 endocytosis, we
282 introduced point mutations either in both PPxY motifs (TXNIP$^{PPCY331AACA,\ PPTY375AATA}$,
283 hereafter TXNIP^{PPxYmut}), or only in the first PPxY motif (TXNIP^{PPCY331AACA}, hereafter
284 TXNIP^{PPxY331}) and expressed these mutants in TXNIP^{KO} RPE1 cells. The protein levels of the
285 PPxY mutants were higher compared to endogenous TXNIP (Figure 4b and Supplementary
286 Figure 3a), yet the endocytic downregulation of SLC7A5-SLC3A2 was blocked (Figure 4b and
287 Supplementary Figure 3a) and SLC3A2 remained at the PM in response to serum starvation
288 (Figure 4c, d and Supplementary Figure 3a - c).
289 A fraction of ALFA-TXNIP^{PPxY331} localized to the PM in proliferating cells, similar to wildtype
290 ALFA-TXNIP. In response to serum starvation, the signal for ALFA-TXNIP^{PPxY331} persisted at
291 the PM, where it co-localized with SLC3A2, while ALFA-TXNIP was cleared from the PM
292 together with SLC3A2 (Figure 4e). These results indicated that the endocytic downregulation
293 of SLC7A5-SLC3A2 required the PPCY motif at position 331 of TXNIP.
294 To examine the capacity of TXNIP and its PPxY motif to interact with different HECT-type
295 ubiquitin ligases, we co-expressed ALFA-TXNIP or ALFA-TXNIP^{PPxY331} with YFP-NEDD4,
296 -ITCH, -WWP1, WWP2, and -HECW1 [41, 42] in HEK293T cells. A robust interaction of ALFA-
297 TXNIP with YFP-NEDD4, YFP-WWP1 and YFP-WWP2 was detected (Figure 4f and
298 Supplementary Figure 3d), which required the PPCY motif at position 331 in TXNIP (Figure
299 4f and Supplementary Figure 3d). The interaction of TXNIP appeared to be weaker with

300 HECW1, and the interaction with ITCH was barely detected (Supplementary Figure 3d). It
301 seemed that the PPCY motif at position 331 rendered TXNIP capable to interact with different
302 HECT type ubiquitin ligases.
303 To examine if entry into quiescence induced TXNIP mediated ubiquitination of SLC7A5, we
304 replaced endogenous SLC7A5 with C-terminally ALFA-tagged SLC7A5 (SLC7A5-ALFA).
305 Therefore, we generated SLC7A5^{KO} cells (using CRISPR/Cas9 mediated gene editing,
306 Supplementary Figure 3e), as well as SLC7A5^{KO} TXNIP^{KO} double knock out cells and stably
307 over-expressed SLC7A5-ALFA. To detect ubiquitination, SLC7A5-ALFA was
308 immunoprecipitated under denaturing conditions (1% SDS) before and after 7 h of serum
309 starvation. Polyubiquitination of SLC7A5-ALFA was detected under steady state conditions,
310 and appeared to slightly increase 7 h after serum starvation. The polyubiquitination of SLC7A5-
311 ALFA was markedly reduced in the TXNIP^{KO} cells (Figure 4g). Hence, TXNIP seemed to be
312 required for the efficient polyubiquitination of SLC7A5-ALFA.
313 Taken together, these findings suggested that TXNIP used its PPxY motif to interact with
314 HECT-type ubiquitin ligases for the efficient ubiquitination of SLC7A5-SLC3A2, leading to
315 endocytic downregulation.
316
317 **AKT signaling controls TXNIP mediated downregulation of SLC7A5**
318 Earlier work demonstrated that AKT directly phosphorylated TXNIP on serine 308 to inhibit
319 endocytosis of SLC2A1 and increase glucose uptake [26]. To examine if AKT also controlled the
320 endocytic downregulation of SLC7A5-SLC3A2, we treated RPE1 cells with the AKT inhibitor
321 MK2206 (MK). MK2206 treatment caused the endocytic downregulation of the SLC7A5-
322 SLC3A2 heterodimer (Figure 5a, lane 3 and Supplementary Figure 4a), but not of SLC1A5
323 (Supplementary Figure 4a). Inhibition of MEK with PD0325901 (PD) triggered the selective
324 endocytic downregulation of SLC1A5, but not of SLC7A5-SLC3A2 (Figure 5a, lane 4 and
325 Supplementary Figure 4a). These results suggested that distinct mitogenic signaling cascades
326 regulated the PM levels of different AA transporters, with AKT controlling SLC7A5-SLC3A2
327 endocytosis.
328 To test if AKT controlled SLC7A5 endocytosis via TXNIP, we treated RPE1 WT and TXNIP^{KO}
329 cells with MK2206. In the TXNIP^{KO} cells, endocytosis and degradation of SLC3A2 was
330 blocked in response to MK2206 treatment, suggesting that TXNIP functioned downstream of
331 AKT to mediate SLC7A5-SLC3A2 endocytic degradation (Figure 5b, c, lane 1 – 3 and 13 -
332 15). Consistently, the phospho-mimetic TXNIP^{S308D} mutant blocked SLC3A2 endocytosis in
333 response to serum starvation or AKT inhibition, while the non-phosphorylatable TXNIP^{S308A}

334 mutant allowed SLC7A5-SLC3A2 endocytic degradation (Figure 5b, c). These findings were
335 corroborated by cell surface FACS analysis of SLC3A2 (Figure 5d and Supplementary Figure
336 4b).
337 TXNIP forms a disulfide bound (S-S) via cysteine 247 to inhibit TRX (thioredoxin) activity
338 [23,24]. To test the role of the S-S between TXNIP and TRX in SLC7A5-SLC3A2 endocytosis,
339 we generated mutant $TXNIP^{C247S}$, which no longer formed a S-S bridge with TRX [43]. The
340 expression of $TXNIP^{C247S}$ in $TXNIP^{KO}$ cells rescued the endocytic degradation of SLC7A5-
341 SLC3A2, similar to WT TXNIP (Figure 5b - d). Thus, SLC7A5 endocytosis was independent
342 of the ability of TXNIP to form disulfide bridges with TRX.
343 These results demonstrated that AKT mediated phosphorylation of TXNIP at serine 308
344 inhibited SLC7A5-SLC3A2 endocytosis, while reduction of AKT signaling enabled TXNIP
345 mediated SLC7A5-SLC3A2 endocytic degradation.
346
347 **TXNIP mediated downregulation of SLC7A5 was essential to adjust intracellular AA**
348 **levels and metabolic signaling in cells entering quiescence**
349 Our results so far linked growth factor signaling via AKT with the TXNIP mediated control of
350 AA acquisition via SLC7A5-SLC3A2. To directly test whether TXNIP mediated endocytosis
351 of SLC7A5-SLC3A2 adjusted AA uptake in cells entering quiescence, we measured the cellular
352 uptake of [^{3}H]-leucine. In response to serum starvation, WT cells downregulated [^{3}H]-leucine
353 uptake, while $TXNIP^{KO}$ cells did not reduce [^{3}H]-leucine uptake (Figure 6a). Upon JPH203
354 treatment, a selective inhibitor of SLC7A5 [44], the uptake of [^{3}H]-leucine was blocked in WT
355 cells and $TXNIP^{KO}$ cells (Figure 6a), suggesting that SLC7A5 was the main transporter for
356 leucine in RPE1 cells. Consistently, in $SLC7A5^{KO}$ cells, the uptake of [^{3}H]-leucine was strongly
357 impaired (Supplementary Figure 5a).
358 To assess the effect of SLC7A5 downregulation or the lack thereof on intracellular free AA
359 levels, we used quantitative mass spectrometry. We quantified free levels of 17 different
360 proteinogenic AA in WT, $TXNIP^{KO}$ and $SLC7A5^{KO}$ RPE1 cells. In $SLC7A5^{KO}$ cells the
361 intracellular levels of L, I, W, V, F, Y were low under all conditions (Figure 6b), with exception
362 for M, which was upregulated (Supplementary Figure 5b). These LNAAs are known substrates
363 of SLC7A5 [1] (Figure 6b). In WT cells, the free levels of most these AAs (L, I, W, V, F, Y)
364 decreased (Figure 6b). In contrast, the levels of L, I, W, V, F, Y were lower in growing
365 $TXNIP^{KO}$ cells, and they did not decrease when $TXNIP^{KO}$ cells entered quiescence (Figure 6b).
366 Neither loss of SLC7A5 nor loss of TXNIP affected the levels K, R, S, E, Q, P, G, A

367 (Supplementary Figure 5b, c). Taken together, these data indicated that the loss of TXNIP
368 affected the ability of cells to control SLC7A5 dependent AA transport.
369 To characterize the consequence resulting from the failure to adjust AA uptake in TXNIP^{KO}
370 cells, we determined how mTORC1 dependent translational control was affected. In quiescent
371 WT cells, phosphorylation of S6K on threonine 389 was reduced compared to proliferating
372 cells, as was phosphorylation of the S6K substrate S6 on serine 240/244, in keeping with lower
373 mTORC1 activity (Figure 6c, lane 3 and 4, Figure 6d, e). In TXNIP^{KO} cells, S6K and S6
374 phosphorylation also decreased, but remained higher compared to WT cells (Fig 6c, lane 1 and
375 2, Figure 6d, e), indicating elevated mTORC1 activity. Another important mode for
376 translational control is eIF2α phosphorylation at serine 51 by GCN2 (but also other kinases of
377 the integrated stress response) in response to lower AA levels. In quiescent WT cells,
378 eIF2α phosphorylation at serine 51 increased (Figure 6c, lane 3 and 4, Figure 6f). However, in
379 growing TXNIP^{KO} cells, eIF2α phosphorylation appeared to be slightly elevated but did not
380 further increase, as these cells transitioned into quiescence (Figure 6c, lane 1 and 2, Figure 6f).
381 It seemed that TXNIP mediated SLC7A5-SLC3A2 endocytosis was required to decrease AA
382 uptake in quiescence, which helped to change signaling towards the translation machinery,
383 possibly to adapt translation.
384 In line with this concept, [^{35}S]-methionine and [^{35}S]-cysteine incorporation into newly
385 synthesized proteins remained higher in quiescent TXNIP^{KO} cells, and also appeared to increase
386 faster after the re-addition of serum (Figure 6d). The increased translation in the TXNIP^{KO} cells
387 required SLC7A5, because it was no longer observed in TXNIP^{KO} SLC7A5^{KO} double mutant
388 cells (Figure 6g).
389 We concluded that TXNIP mediated endocytosis of SLC7A5-SLC3A2 reduced the uptake of
390 LNAAs such as L, I, W, V, F, Y, which in turn lowered the free intracellular levels of these
391 AA, thereby helping cells to reduce mTORC1 signaling and to dampen translational activity.
392
393 **TXNIP mediated endocytic degradation of SLC7A5 restrains cell proliferation**
394 Finally, we determined how the TXNIP mediated regulation of SLC7A5 and AA uptake
395 contributed to cell cycle progression during entry into and exit from quiescence. Therefore, we
396 compared the DNA content of WT, TXNIP^{KO} and TXNIP^{KO} cells which re-expressed TXNIP
397 during entry and exit from serum starvation induced quiescence (Figure 7a).
398 In a growing cell population and 24 h after serum starvation, the DNA content of WT, TXNIP^{KO}
399 and rescued cells was similar (Figure 7a, timepoint 0 h and 24 h). Interestingly, 24 h after serum
400 re-addition (timepoint 48 h), a larger fraction of the TXNIP^{KO} cells (35%, ± 1%) had already

401 reached the G2/M phase of the cell cycle. In comparison, only 13% (± 10%) of WT cells or
402 17% (± 12%) of TXNIP^{KO} cells re-expressing TXNIP reached G2/M phase and more cells (35%
403 ± 10% of WT cell and 25% ± 11% of rescued TXNIP^{KO}) were still in S-Phase (Figure 7a).
404 Consistent with a faster cell cycle progression of TXNIP^{KO} cells during exit from quiescence,
405 these cells resumed cell proliferation faster compared to WT cells, which was dependent on
406 SLC7A5 (Figure 7b). Moreover, the overall cell proliferation rate of TXNIP^{KO} cells or of
407 TXNIP^{KO} cells expressing TXNIP^{S308D} was increased compared to WT or TXNIP^{KO} cells
408 expressing TXNIP or TXNIP^{S308A} (Figure 7c). Again, the increased proliferation of TXNIP^{KO}
409 cells was dependent on SLC7A5, since the double knock out TXNIP^{KO} SLC7A5^{KO} grew slower,
410 similar to SLC7A5^{KO} cells (Figure 7c).
411 Taken together, our results demonstrated that TXNIP interacted with HECT-type ubiquitin
412 ligases to selectively degrade SLC7A5-SLC3A2 in cells entering quiescence, thereby reducing
413 AA uptake. This process not only contributed to reduce translation, but also restrained cell cycle
414 progression during the exit from quiescence and limited overall cell proliferation (see Figure
415 7d model). This mechanism was only licensed upon serum removal and repressed by growth
416 factor signaling through AKT.
417

418 **Discussion**

419 Our work establishes a central role for TXNIP in a functional feedback loop that links growth
420 factor signaling, AA homeostasis and metabolic signaling for translational control during
421 cellular transitions between proliferation and quiescence, with potential relevance for human
422 health. In particular, we made progress toward understanding how growth signaling regulates
423 TXNIP mediated endocytosis of SLC7A5-SLC3A2 and hence, the acquisition of LNAAs for
424 metabolic scaling in growing and quiescent cells. The framework of our model (Figure 7d) is
425 based on the following results: (1) Human cells that enter quiescence downregulate AA uptake,
426 in part, by selective endocytosis of the AA transporters; (2) the α-arrestin TXNIP mediates the
427 selective endocytosis of SLC7A5-SLC3A2; (3) TXNIP mediated endocytosis is suppressed in
428 growing cells by AKT signaling downstream of growth factor receptors and (4) TXNIP
429 mediated SLC7A5-SLC3A2 endocytosis helps to lower AA uptake, translation and thereby
430 restrains cell proliferation. (5) These processes contribute to metabolic homeostasis in humans.
431 A novel loss-of-function mutation in TXNIP, that impairs AA endocytosis, causes a rare
432 metabolic disease.
433 Together with a previous report on three siblings from a single consanguineous family that were
434 homozygous for a loss-of-function frameshift variant c.174_175delinsTT [28], our data suggest

435 TXNIP deficiency as a novel inherited metabolic disease with specific metabolic alterations,
436 that appear associated with neonatal lactic acidosis, recurrent hypoglycaemia, and specific
437 anomalies in AA metabolism, although full the spectrum of associated clinical manifestations
438 remains uncertain. Similar to our patient, the three siblings presented with lactic acidosis in the
439 neonatal period, which was treated with long-term dichloroacetic acid (DCA). Rather than
440 directly clearing lactate from serum, DCA inhibits pyruvate dehydrogenase kinase to stimulate
441 pyruvate dehydrogenase activity and oxidative decarboxylation of pyruvate, resulting in
442 reduced serum lactate levels [45 46]. Two of the three affected children had normal development
443 during childhood; one child, which also suffered from recurrent hypoglycaemia, had neonatal
444 muscular hypotonia and failure to thrive, and was under investigation for autism spectrum
445 disorder, similar to our patient. Our patient additionally has an increasing frequency of epileptic
446 seizures. The three siblings developed low plasma methionine concentrations. No other AA
447 anomalies were specified in the previous report except for a transient general
448 hyperaminoaciduria in one child [28]. The detailed metabolic investigations in our case revealed
449 relative normal methionine levels, but identified other specific AA alterations in line with
450 impaired SLC7A5 endocytosis in the case of complete TXNIP loss. How these metabolic
451 defects are linked to other clinical manifestations such as possible autism and the severe
452 epileptic developmental disorder in our patient, remains to be investigated. We speculate that
453 these feature could be related to role of SLC7A5 in neurons and in the blood brain barrier [47,48].
454 Yet, the patient phenotype appears to be variable in severity and not fully penetrant. Hence,
455 loss of TXNIP alone is likely to be insufficient and other genetic or non-genetic factors (e.g.
456 diet) that are not yet known, must be involved.
457 Several studies in mice show that TXNIP is important during the transition between fed and
458 fasted states, which was attributed to its role in glucose and energy metabolism [49-52]. Our
459 findings imply that at least some of the described TXNIP dependent effects on glucose
460 homeostasis might also be linked to TXNIP dependent regulation of SLC7A5-SLC3A2 and the
461 regulated import of LNAAs as cells enter and exit quiescence.
462 While it is clear how proliferating cells benefit from the upregulation of SLC7A5-SLC3A2, it
463 is less clear how quiescent cells could profit from the downregulation of SLC7A5-SLC3A2.
464 One rational for the selective endocytosis of this AA transporter could be that the cellular
465 demand for essential AAs must be matched to lower rates of protein translation in quiescent
466 cells. In line with this concept, also quiescent mammary epithelial cells reduced levels of V, L,
467 I and Q [53]. Similar results were obtained in a non-malignant murine pro-B lymphocyte cell line
468 (FL5.12), in which the abundance of SLC3A2 at the plasma membrane was regulated by the

469 presence of growth factors [54]. In those cells, the consumption rate of essential AAs was
470 decreased in G0 arrest and increased upon re-entry into the cell cycle [55]. Hence, the
471 downregulation of AA transporters provide means to avoid an excess/imbalance of free
472 intracellular AAs which facilitates the controlled decrease of mTORC1 signaling and the
473 ensuing reduction of translation rates, possibly in conjugation with the integrated stress
474 response. Thereby, the TXNIP mediated selective downregulation of SLC7A5-SLC3A2 and
475 the ensuing decreased import of essential AAs, helps to promote the switch from anabolic to
476 catabolic metabolism. Moreover, the downregulation of AA transporters upon entry into
477 quiescence might also contribute to the barrier for cellular transformation [5 56-58].
478 TXNIP was specifically required for the endocytosis of SLC7A5-SLC3A2, but not for the
479 endocytosis of SLC7A11-SLC3A2. How TXNIP interacts specifically with SLC7A5-SLC3A2
480 remains unclear at the moment. Yet it is clear that TXNIP requires its first PPCY motif (331)
481 to interact with several different HECT type ubiquitin ligases, and this interaction is required
482 for the downregulation of SLC7A5. In line with our results, SLC7A5 was shown to be
483 ubiquitinated on N-terminal lysine residues by Nedd4-2 upon protein kinase C (PKC) activation
484 and mTORC1 inhibition [59,60].
485 We conclude that the role of TXNIP in controlling the abundance of SLC7A5-SLC3A2 at the
486 PM is important to match AA uptake with metabolic needs in proliferating and quiescent cells.
487 In the future it will be important to understand how these cellular functions of TXNIP and the
488 loss thereof translate into complex metabolic phenotypes of human patients with loss of TXNIP
489 variants.
490

Acknowledgments

We thank the patient and his family. We are grateful to Hemmo Meyer and Simona Polo for providing the YFP-tagged HECT type ubiquitin ligases. This research was funded in part by the Austrian Science Fund (FWF) (10.55776/P35874, 10.55776/P34907, 10.55776/FG20 to DT, 10.55776/P35832, 10.55776/P36600 to HF, 10.55776/P36925 to VR, 10.55776/P30196 to SH, and 10.55776/DOC82 to FH, DT, LAH, KT and MA). JK is a recipient of a DOC Fellowship of the Austrian Academy of Sciences. KT acknowledges support from the DFG (German Research Foundation, project No TH 1358/3e2), the MESI-STRAT project (grant agreement No 754688) which has received funding from the European Union's Horizon 2020 research and innovation programme, and from the European Union European Research Council (ERC AdG BEYOND STRESS, grant agreement No 101054429) which has received funding from the European Union's Horizon Europe research and innovation programme. For open access purposes, the author has applied a CC BY public copyright license to any author accepted manuscript version arising from this submission.

Material and methods

Cell culture

Patient-derived primary fibroblasts were cultured from skin biopsies. Control fibroblasts were obtained from a male, born in 2000 (WT#1) and from a male, born in 2015 (WT#2). RPE1, HEK293T, A549, H460, HCC4006, primary human fibroblasts and MEF (mouse embryonic fibroblasts) [61] were cultured in DMEM containing high glucose (4.5 g/L) (Sigma-Aldrich, #D6429), supplemented with 1% (vol/vol) penicillin/streptomycin (Sigma-Aldrich, #P0781) and 10% (vol/vol) FBS (fetal bovine serum) (Sigma-Aldrich, #S0615) at 37°C, in 5% CO_2 and 98% humidity. H2228, H226, H520 and H1299 cells were cultured in RPMI 1640, glutamax supplement medium (Thermo Fisher, Gibco, # 61870044) supplemented with 1% (vol/vol) penicillin/streptomycin (Sigma-Aldrich, #P0781) and 10% (vol/vol) FBS (Sigma-Aldrich, #S0615) under the same culture conditions. Cells were passaged before reaching confluency by incubation in 1x PBS (phosphate-buffered saline, 8 g/L NaCl, 0.2 g/L KCl, 1.15 g/L Na_2HPO_4, 0.2 g/L KH_2PO_4) and 1x trypsin-EDTA solution (Sigma-Aldrich, #T4174). Cells were resuspended in growth medium and re-seeded at a 1:5 to 1:10 ratio. Cells were regularly tested negative for mycoplasma.

The AKT inhibitor MK2206 (Enzo Life Sciences, #ENZ-CHM164-0005), dissolved in DMSO (Sigma-Aldrich, #D2650), was used at a final concentration of 1 μM. The MEK inhibitor

526 PD0325901 (Absource, #S1036), dissolved in DMSO, was used at a final concentration of 5
527 µM. The SLC7A5 inhibitor JPH203 (also KYT-0353, Selleckchem, #S8667), dissolved in
528 DMSO, was used at a final concentration of 10 µM. Chloroquine (Sigma-Aldrich, #C6628) was
529 dissolved in Millipore H_2O and used at a final concentration of 12.5 µM. To inhibit dynamin
530 mediated endocytosis, dynasore hydrate (Sigma-Aldrich, #D7693) was used as previously
531 described [31] at a final concentration of 20 µM.
532
533 To maintain cells in proliferation (control cells, defined as "+ serum"), they were cultured in
534 DMEM containing 4.5 g/L glucose and all AAs, (Sigma-Aldrich, #D6429), supplemented with
535 1% (vol/vol) penicillin/streptomycin (Sigma-Aldrich, #P0781) and 10% (vol/vol) FBS (Sigma-
536 Aldrich, #S0615). To induce quiescence, cells were washed with 1x PBS and cultured in
537 DMEM containing 4.5 g/L glucose and all AAs, supplemented with 1% penicillin/streptomycin
538 but without FBS for 24 h (referred to as serum starvation, "- serum").
539
540 **Proliferation assay**
541 A similar cell number (>20000 cells) was seeded onto 6-well plates (day 0). Cells were
542 harvested daily by trypsinization. The cell number was measured daily using a CASY Cell
543 Counter and Analyzer (OMNI Life Science) for 4 days. The cell proliferation index was
544 calculated as described before [62]. The fold increase was calculated by normalizing to the cell
545 number obtained 24 h after seeding (day 1).
546
547 For measuring cell proliferation in an automated manner, 50000 cells were seeded onto a 6-
548 well plate and cultured at standard cell culture conditions. Cells were set on serum free medium
549 24 h after seeding and refed after 48 h of serum starvation. Cell proliferation was tracked using
550 a Sartorius IncuCyte® S3 Live Cell Imaging System and confluency measurement was
551 performed every 4 h for 5 days. Data were acquired and analyzed using the Sartorius IncuCyte®
552 S3 software version 2022B.
553
554 **Preparation of whole cell protein extracts, SDS-PAGE and Western Blot analysis**
555 Cells were washed in 1x cold PBS, harvested using a cell scraper and pelleted at 13.000 rpm
556 for 5 min at 4°C. The cell pellets were resuspended in cold RIPA lysis buffer (50 mM Tris-HCl
557 pH 7.5, 150 mM NaCl, 1% NP-40, 2 mM EDTA pH 8, 0.1% SDS, 0.5% sodium deoxycholate)
558 or lysis buffer (50 mM Tris-HCl pH 7.5, 150 mM NaCl, 1% Triton X-100, 10% glycerol, 0.5
559 mM EDTA), supplemented with 50 mM NaF, 10 µg/mL leupeptin, 1 mM pefablock, 1 µg/mL

560 pepstatin, 10 µg/mL aprotinin, 2 mM Na_3VO_4. Cells were lysed for 30 min on ice, centrifuged
561 at 13.000 rpm for 10 min at 4°C and the cleared lysate was obtained. Protein concentration was
562 measured using Micro BCA Protein Assay Kit (Thermo Scientific, #23235) according to the
563 manufacturer's instructions. 20 µg protein was supplemented with 5x Urea sample buffer (8 M
564 Urea, 5% SDS, 40 mM Tris pH 6.8, 0.1 mM EDTA, 0.4 mg/mL bromphenol blue, 1% final β-
565 mercaptoethanol) at 1x final concentration. Lysates were separated by SDS-PAGE. Proteins
566 were transferred onto polyvinylidene fluoride (PVDF) membranes (Amersham Hybond PVDF,
567 #10600023 – 0.45 µm) using a wet transfer system (Bio-Rad) at constant 80V for 2 h (1x
568 transfer buffer: 20% methanol, 25 mM Tris-HCl, 192 mM glycine). Membranes were blocked
569 in 5% milk in Tris-buffered saline buffer (TBS, 0.5 M NaCl, 20 mM Tris, pH 7.5) with 0.05%
570 Tween 20 (TBS-T) and probed with the respective antibodies over night at 4°C. The membranes
571 were washed with TBS-T and probed with the respective horseradish peroxidase-linked
572 secondary antibodies (1:5000 dilution) for 1 h at RT. After washing with TBS-T, the membrane
573 was incubated with WesternBright Chemiluminescence substrate solution (Advansta) (Biozym,
574 #541005X). The chemiluminescence signal was detected either on X-ray films or with a CCD-
575 Camera (Fusion FX, Vilber Lourmat). The signal was quantified with ImageJ and normalized
576 to GAPDH. To quantify the phosphorylation of proteins, the signals were normalized to the
577 unphosphorylated total protein levels.
578
579 **Denaturing SLC7A5-ALFA immunoprecipitation**
580 Immunoprecipitation of SLC7A5-ALFA under denaturing lysis conditions was adopted from
581 [63]. Cells expressing SLC7A5-ALFA were either grown in growth medium (+ serum) or serum
582 starved for 7 or 8 h (- serum). Cells were washed with 1x PBS and harvested. Cell pellets were
583 resuspended in lysis buffer I (50 mM Tris pH 8, 150 mM NaCl, 50 mM NaF, 5 mM EDTA, 1%
584 SDS, 10 nM NEM, 10 µg/mL leupeptin, 1 mM pefablock, 1 µg/mL pepstatin, 10 µg/mL
585 aprotinin) and incubated 30 min at RT. Protein concentration was measured using Micro BCA
586 Protein Assay Kit (Thermo Scientific, #23235) according to the manufacturer's instructions.
587 Equal amounts of proteins were diluted by addition of 800 µl lysis buffer II (50 mM Tris pH 8,
588 150 mM NaCl, 50 mM NaF, 5 mM EDTA, 1% Triton X-100, 10 nM NEM, 10 µg/mL leupeptin,
589 1 mM pefablock, 1 µg/mL pepstatin, 10 µg/mL aprotinin). Samples were subjected to
590 immunoprecipitation. Beads (ALFA Selector ST, NanoTag Biotechnologies, #N1516) were
591 equilibrate in washing buffer I (50 mM Tris pH 8, 150 mM NaCl, 1% Triton X-100). Cell
592 suspension and beads were incubated rotating at 4°C for 3 h. Beads were recovered with a
593 magnetic rack and washed twice with washing buffer I and three times with washing buffer II

594 (50 mM Tris pH 8, 300 mM NaCl, 1% Triton X-100). Proteins were eluted with 5x SDS sample
595 buffer (250 mM Tris-HCl pH 6.8, 10% SDS, 50% glycerol, 10% β-mercaptoethanol) and
596 denatured for 10 min at 95°C. For detection of ubiquitinated proteins, samples were separated
597 by SDS-PAGE. Proteins were transferred onto PVDF membranes (Amersham Hybond PVDF,
598 #10600023 – 0.45 µM (300mm)) using a wet transfer system (Bio-Rad) at constant 80V for 2
599 h. After transfer, the membrane was blocked with 10% BSA in 0.45% Tween 20 for at least 1
600 h and incubated with anti-ubiquitin antibody (Santa Cruz, ##3936S) overnight in 10% BSA
601 blocking solution.
602
603 **Non-denaturing ALFA-TXNIP immunoprecipitation**
604 Non-denaturing immunoprecipitation of ALFA-TXNIP was adopted from [27]. Briefly, cells were
605 washed with 1x PBS and harvested by scraping. Cells were lysed in lysis buffer (30 mM Tris
606 pH 7.5, 120 mM NaCl, 20 mM NaF, 0.5% octyl-β-D-glucopyranosid) (Sigma-Aldrich,
607 #O8001) and protease inhibitors (10 µg/mL leupeptin, 1 mM pefablock, 1 µg/mL pepstatin, 10
608 µg/mL aprotinin, 2 mM Na_3VO_4). Cells were lysed for 30 min on ice, centrifuged at 13.000
609 rpm, at 4°C for 10 min and cleared lysate was obtained. Protein concentration was measured
610 using Micro BCA Protein Assay Kit (Thermo Scientific, #23235) according to the
611 manufacturer's instructions. Equal amounts of proteins were subjected to immunoprecipitation.
612 Beads (ALFA Selector ST, NanoTag Biotechnologies, #N1516) were equilibrated in lysis
613 buffer. Cell suspension and beads were incubated rotating at 4°C for 3 h. After incubation beads
614 were washed three times for 10 minutes at 4 °C using wash buffer (30 mM Tris pH 7.5, 150
615 mM NaCl, 0.1% octyl-β-D-glucopyranosid). Proteins were eluted in 100µl 2x Urea sample
616 buffer at 42°C for 30 min.
617
618 **Genetic modifications and cloning**
619 Genetic modifications were performed by PCR using standard techniques or by using the
620 Gateway cloning method (Thermo Fisher Scientific) according to manufacturer's instructions.
621 All plasmids and primers used in this study are listed in Supplementary Table 3 and
622 Supplementary Table 4. The sequence-verified plasmids were then used for lentiviral
623 transduction of RPE1 cells. To generate virus particles, HEK293T cells were seeded in a 6-well
624 tissue culture plate and transfected with 2 µg lentiviral vector containing the gene of interest
625 together with virus packing vectors (1 µg pVSV-G and 1 µg psPAX2) using polyethylenimine
626 (PEI, Polyscience, #23966-100) as transfection reagent. 4 - 8 h after transfection, the medium
627 was changed. Virus particle-containing medium was collected from the HEK293T cells 48 h

628 and 72 h after transfection and was used to infect RPE1 cells. Polybrene was added to the virus-
629 particle-containing medium to help lentivirus integration (1:500 dilution, Sigma-Aldrich,
630 #107689). After 10 days of selection with 1 µg/mL blasticidin (InvivoGen, #ant-bl-5b), the
631 efficacy of the virus transduction was tested via SDS-PAGE and Western Blot analysis.
632
633 Genetic deletion using CRISPR/Cas9 mediated gene editing was performed as previously
634 described [64]. For CRISPR/Cas9-mediated depletion, guide RNA (gRNA) targeting primers for
635 SLC7A5 (5'-caccgCGTGAACTGCTACAGCGTGA -3' and 5'-aaac
636 TCACGCTGTAGCAGTTCACGc -3') and TXNIP (5'-
637 caccgGTAAGTGTGGCGGGCCACAA-3' and 5'-aaacTTGTGGCCCGCCACACTTACc-3').
638 RPE1 cells were transiently transfected with the gRNA-containing pSpCas9(BB)-2A-GFP
639 plasmid (Addgene, #48138) using Lipofectamin LTX reagent (Thermo Scientific, #15338-100)
640 according to the manufacturer's protocol. 24 h after transfection, GFP-positive, transfected cells
641 were enriched by flow cytometry (BD FACSAria III Cell Sorter, BD Biosciences). The sorted
642 cell suspension was used for the generation of single cell clones. Depletion efficiency was
643 verified by PCR using specific primers and Western Blot analysis.
644
645 For the transient transfection of HEK293T Lipofectamine LTX & Plus reagent (Thermo
646 Scientifc, #15338100) was used according to the manufacturer's protocol. HEK293T cells were
647 seeded in a 10 cm dish. At around 80% confluency, 16 µg of the respective plasmids were
648 diluted in 500 µl of OptiMEM (Thermo Scientific, #31985062) in the presence of 48 µl of LTX-
649 and 16 µl of Plus-reagent for the transfection. The transfected cells were incubated for 4 h
650 before the transfection medium was discarded and replaced with 10 ml of fresh DMEM. After
651 that, cells were incubated for 24 h under standard conditions.
652
653 **Immunofluorescence microscopy**
654 Cells were grown on 12 mm glass coverslips (Hartenstein GmbH, #DKR1) and fixed with 4%
655 paraformaldehyde (PFA) for 10 - 15 min at RT. Immunofluorescence staining of SLC3A2 and
656 ALFA-tagged proteins was performed as described previously [65]. Briefly, cells were
657 permeabilized and blocked in blocking buffer (10% FBS, 0.3% saponin (BioChemika, #84510),
658 sodium azide (0.02% final) in 1x PBS) for 30 min at 37°C. Cells were incubated with mouse
659 anti-SLC3A2 (BD Pharmingen, #556074) or rabbit anti-ALFA (NanoTag Biotechnologies,
660 #N1581) in a 1:100 dilution in blocking buffer overnight at 4°C. For double-staining with
661 LAMP1, cells were simultaneously incubated with rabbit anti-LAMP1 (Cell Signaling, #9091)
662 in a 1:800 dilution in blocking buffer. Cells were washed once with wash solution (0.03%

663 saponin, sodium azide (0.02% final) in 1x PBS), following three washing steps with PBS and
664 incubated with Alexa Fluor 488 goat anti-mouse IgG (Invitrogen, #A11001) and Alexa Fluor
665 568 goat anti-rabbit IgG (Invitrogen, #A11011) in a 1:500 dilution in blocking buffer for 1 h at
666 RT.
667
668 For immunofluorescence labeling of SLC1A5, cells were permeabilized in in 0.2% Triton X-
669 100 (Thermo Scientific, #28314) in PBS for 5 min and blocked in blocking buffer (2% gelatin,
670 150 mM NaCl, 10 mM Pipes pH 6.8, 5 mM EGTA, 5 mM glucose, 5 mM $MgCl_2$, 50 mM
671 NH_4Cl) for 1 h at RT. Cells were incubated with rabbit anti-SLC1A5 (Sigma-Aldrich,
672 #HPA035240) in a 1:50 dilution in blocking buffer for 1 h at RT. For double-staining with
673 LAMP1, cells were simultaneously incubated with mouse anti-LAMP1 (DSHB, #H4A3-S) in
674 a 1:50 dilution in blocking buffer. Cells were washed with PBS and incubated with Alexa Fluor
675 488 goat anti-rabbit IgG (Invitrogen, #A11008) and Alexa Fluor 568 goat anti-mouse IgG
676 (Invitrogen, #A11031) in a 1:500 dilution in blocking buffer for 1 h at RT.

677 For immunofluorescence labeling of SLC2A1, cells were permeabilized and blocked in
678 blocking buffer (2% gelatin, 150 mM NaCl, 10 mM Pipes pH 6.8, 5 mM EGTA, 5 mM glucose,
679 5 mM $MgCl_2$, 50 mM NH_4Cl) containing 0.025% saponin (BioChemika, #84510) for 1 h at RT.
680 Cells were incubated with rabbit anti-SLC2A1 (Merck, #07-1401) in a 1:200 dilution in
681 blocking buffer for 1 h at RT. Cells were washed with PBS and incubated with Alexa Fluor 488
682 goat anti-rabbit IgG (Invitrogen, #A11008) in a 1:500 dilution in blocking buffer for 1 h at RT.
683 Cells were washed with 1x PBS, incubated with DAPI (Sigma-Aldrich, #D9542) in a 1:20000
684 dilution in 1x PBS and mounted in Mowiol (Sigma-Aldrich, #81381).

685 Confocal microscopy was performed on a LSM980 AiryScan 2 (ZEISS). Confocal Z-series
686 stack (step size 0.22 µm) images were acquired using the AiryScan detector, a LD LCI Plan-
687 Apochromat 63x / 1.2 with glycerol immersion objective (ZEISS) and the 405 nm, 488 nm and
688 561 nm laser lines. To compare signals of a protein of interest in proliferating, quiescent or
689 treated cells, laser settings were kept constant while imaging both conditions. The ZEISS Zen
690 3.5 software was used as recording software and for processing of the raw images (AiryScan
691 processing). Brightness and contrast were adjusted using ImageJ software. For merged images,
692 the levels of red, green and blue channels were separately adjusted.
693
694 **Cell surface staining of SLC3A2 and FACS analysis**

695 To measure the difference in surface staining of SLC3A2 between proliferating and quiescent
696 cells, cells were either grown in growth medium or serum starved for 24 h before the
697 experiment. The staining was performed as previously described [65]. Cells were washed with
698 PBS, trypsinized and resuspended in FACS buffer (10% FBS in 1x PBS) containing anti-
699 SLC3A2 antibody (BD Pharmingen, #556074) at a dilution of 1:100. The antibody was
700 incubated for 30 min on ice. Cells were centrifuged at 1000 rpm for 5 min at 4°C and
701 resuspended in FACS buffer containing Alexa Fluor 488 goat anti-mouse IgG (Invitrogen,
702 #A11001) at a dilution of 1:500. The antibody was incubated for 30 min on ice in the dark.
703 Cells were centrifuged at 1000 rpm for 5 min at 4°C and resuspended in 200µl FACS buffer.
704 The fluorescence intensity was measured by flow cytometry (Attune NxT Flow Cytometer, Life
705 Technologies). For every experiment, more than 3500 cells were analyzed. Flow cytometry
706 analysis was performed with FlowJo software 10.8.1 (BD Life Sciences). Cells were gated by
707 forward versus side scatter (FSC-A vs. SSC-A) to identify cell population, forward scatter width
708 versus forward scatter area (FSC-W vs FSC-A) for doublet exclusion and fluorescence intensity
709 (BL1-A) vs cell count to reflect Alexa-488 signal populations. Unstained cells were excluded
710 from analysis.
711
712 **DNA content for cell cycle analysis of fixed cells stained with propidium iodide (PI)**
713 Cells were washed with PBS and harvested by trypsinization. Cells were centrifuged at 1000
714 rpm for 5 min at 4°C. The pellet was washed in cold PBS. Cells were fixed by resuspending the
715 cells in 1 ml ice cold 70% vol/vol ethanol in PBS. Samples were stored at -20°C for at least 30
716 min. The ethanol was washed away with ice cold PBS twice. Cells were then incubated with
717 propidium iodide (PI) at a final dilution of 1:25 and RNAse A (Thermo Scientific, #EN0531)
718 at a final dilution of 1:100 in PBS, for 30 min at 37°C. The fluorescence intensity was measured
719 by flow cytometry (Attune NxT Flow Cytometer, Life Technologies). For every experiment,
720 more than 1500 cells were analyzed. Data were analyzed using ModFit LT (Verity Software
721 House). Cells were gated by forward versus side scatter (FSC-A vs. SSC-A) to identify cell
722 population. PI-positive cells were gated for doublet exclusion by width vs height (BL3-H vs
723 BL3-W) and fluorescence intensity (BL3-A) vs cell count to reflect PI-positive signal
724 populations.
725
726 RNA was extracted from cells using the RNeasy Mini Kit (Quiagen, #74104) according to the
727 manufacturer's instructions. 800 ng RNA were reverse transcribed into cDNA using the
728 LunaScript RT Super Mix Kit (NEB, #E3010) according to manufacturer's protocol. For

729 mRNA fold regulation analysis, quantitative real-time PCR was performed using gene specific
730 primers listed in Supplementary Table 5. The Biozym Blue S'Green qPCR Kit (Biozym, #F-
731 415S) was used according to manufacturer's protocol. All primers were synthesized by Sigma-
732 Aldrich and diluted in Millipore H_2O to a concentration of 10 µM. Each condition was
733 performed in technical triplicates from three biological replicates. Fold regulation was
734 calculated using the $2^{-\Delta\Delta Ct}$ method and normalized to the housekeeping gene *ribosomal protein*
735 *lateral stalk subunit P0 (RPLP0)*.
736
737 **Uptake of radioactive labeled AAs**
738 To analyze the uptake of L-glutamine, cells were washed with PBS and incubated with 0.3
739 µCi/mL [$^{14}C_5$]-L-glutamine (Hartmann Analytic, #MC1124) in glutamine-free medium
740 (Sigma-Aldrich, #D6546). To analyze the uptake of L-leucine, cells were washed with PBS and
741 incubated with 0.5 µCi/mL [4,5-^{3}H]-L-Leucine (Hartmann Analytic, #MT672E) in AA free
742 medium (USBiological, #D9811-01). The uptake of L-isoleucine was initiated by incubating
743 the cells with 0.005 µCi/mL [$^{14}C_5$]-L-isoleucine (Hartmann Analytic; #MC174) in AA free
744 medium. The uptake was performed for 15 min at 37°C. To stop the reaction, cells were washed
745 twice with ice cold PBS. Cells were harvested by trypsinization and the cell pellet was lysed in
746 100 µl lysis buffer (50 mM Tris-HCl pH 7.5, 150 mM NaCl, 1% NP-40, 2 mM EDTA pH 8,
747 0.1% SDS, 0.5% sodium deoxycholate) for 30 min on ice. Cells debris were removed by
748 centrifugation (13000 rpm, 4°C, 10 min) and the supernatant was analyzed by liquid
749 scintillation counting (LSC-Universal cocktail, Roth, #0016.3; HITACHI AccuFlex LSC-800).
750 AA uptake was calculated as counts per min (cpm) normalized to the protein concentration (µg)
751 of each cleared lysate. Protein concentration was determined by using Micro BCA Protein
752 Assay Kit (Thermo Scientific, #23235) according to the manufacturer's instructions.
753
754 **Glucose uptake assay**
755 The glucose uptake assay was performed as described previously [66]. Briefly, glucose uptake
756 was initiated by adding 2-NBDG (2-(N-(7-Nitrobenz-2-oxa-1,3-diazol-4-yl)amino)-2-
757 deoxyglucose) (AAT Bioquest, #36702, dissolved in DMSO) at a final concentration of 100
758 µM in the respective medium. To inhibit glucose uptake, cells were simultaneously treated with
759 1 mM phloretin (Sigma-Aldrich, #P7912, dissolved in 50% ethanol) for 45 min. After 45 min
760 incubation at 37°C in the dark, cells were washed with ice cold PBS to stop the reaction,
761 trypsinized and resuspended in PBS. Cells were centrifuged at 1000 rpm for 5 min at 4°C and
762 the pellet was resuspended in 200 µl PBS and 10% FBS. The fluorescence intensity was

763 measured by flow cytometry (Attune NxT Flow Cytometer, Life Technologies). For every
764 experiment, more than 5000 cells were analyzed. Flow cytometry analysis was performed with
765 FlowJo software 10.8.1 (BD Life Sciences). Cells were gated by forward versus side scatter
766 (FSC-A vs. SSC-A) to identify cell population, forward scatter width versus forward scatter
767 area (FSC-W vs FSC-A) for doublet exclusion and fluorescence intensity (BL1-A) vs cell count
768 to reflect the uptake of 2-NBDG.
769
770 **Incorporation of ^{35}S labeled L-Cysteine and L-Methionine**
771 150000 cells were seeded and after two days, these cells were left untreated or serum starved
772 for 24 h or serum starved and then refeed for 24 h. Prior to radiolabeling the cells, the serum
773 starved cells were washed with PBS and incubated for 30 min in L-cysteine, L-methionine, L-
774 glutamine free medium (Sigma-Aldrich #D0422), supplemented with 2 mM L-glutamine
775 (Gibco #25030-024) and 1% (vol/vol) penicillin/streptomycin. The proliferating cells were
776 incubated for 30 min in L-cysteine, L-methionine, L-glutamine free medium, supplemented
777 with 2 mM L-glutamine, 10% dialysed FBS (Thermo Fisher Scientific #26400044) and 1%
778 (vol/vol) penicillin/streptomycin. Cells were washed with PBS, brought into suspension using
779 1x trypsin-EDTA solution and resuspended in the corresponding L-cysteine, L-methionine free
780 medium. 17.6 µCi/mL [^{35}S]-methionine [^{35}S]-cysteine (Hartmann Analytic #21635410) was
781 added to the cell suspension for 2 min and quenched with 10 µg/ml cycloheximide. Cell pellets
782 were lysed for 30 min on ice, with RIPA lysis buffer, supplemented with protease inhibitors
783 and 10 µg/ml cycloheximide. Equal amounts of protein were subjected to SDS-PAGE,
784 (de)stained with Coomassie and dried for 1 h at 70°C. The dried gel was exposed to a phosphor-
785 imager for 48 h. Detection of a [^{35}S]-methionine [^{35}S]-cysteine radiogram was performed using
786 a Typhoon FLA 9500 detection system.
787
788 **Mass spectrometry analysis of intracellular free AAs**
789 The analysis of intracellular AAs by mass spectrometry was performed as described previously
790 [67 68]. Briefly, 10^6 cells were seeded and serum starved for 24 h prior the extraction. Then, cells
791 were washed three times with ice cold 1xPBS and extracted by adding 500 µl ice cold methanol
792 (99,9% vol/vol, Fisher Chemicals) and 500 µl cold Millipore H_2O, containing the internal
793 standard (1:100), a stable isotope-labeled canonical AA mix composition (Cambridge Isotope
794 Laboratory, #MSK-CAA-1). Cells were scraped and 500 µl ice cold chloroform (99,9% vol/vol,
795 Sigma-Aldrich, #650498) was added to the cell extracts. Cells were agitated in a tube shaker
796 for 20 min at 1400 rpm at 4°C, followed by centrifugation for 5 min at 16100xg at 4°C. The

797 upper, polar phase was separated, evaporated by using a SpeedVac (Savant SPD111V
798 SpeedVac Concentrator, Thermo Scientific) and stored at -80°C. The interphase was used to
799 determine the protein concentration. Therefore, the interphase was evaporated and the pellet
800 was resuspended in denaturing buffer (1.6 M Urea, 100 mM AmBiCa, pH 8.2) and sonicated
801 for 10 sec to break up protein aggregates. Protein determination was done by using Micro BCA
802 Protein Assay Kit (Thermo Scientific, #23235) according to the manufacturer's instructions.
803 For absolute quantification, AAs were analyzed by targeted LC-MS using mixed-mode
804 chromatography (RP-AEX, reversed phase–anion exchange chromatography) and ultra-high
805 sensitive orbitrap technology (Orbitrap Q Exactive HF-X and Orbitrap Fusion Lumos, both
806 Thermo Scientific), operating in parallel reaction monitoring (PRM) mode. Bioinformatics data
807 processing and statistical analysis was performed using TraceFinder (Thermo Scientific) and
808 in-house R and Python scripts.
809
810 **Statistical analysis and software**
811 Software used in this study, if not already specified, were Affinity Designer Version 1.10.5
812 (Serfi, RRID:SCR_016952), Image J Version 1.53t (RRID:SCR_003070), GraphPad Prism 9
813 Version 9.4.1 (458) (RRID:SCR_002798), Benchling (RRID:SCR_013955), FlowJo Version
814 10.8.1 (RRID:SCR_008520), ModFit LT (RRRID:SCR_016106), Primer3 Version 4.1.0
815 (RRID:SCR_003139), PrimerBank (RRID:SCR_006898), CHOPCHOP
816 (RRID:SCR_015723), ZEISS ZEN Digital Imaging for Light Microscopy Version 3.5
817 (RRID:SCR_013672), and online tools TIDE (tracking of indels by Decomposition) (Brinkman
818 et al. 2014), ICE Analysis online tool (Synthego, v2.0; Synthego, USA) and PrimerQuest™
819 Tool (Integrated DNA Technologies, IDT, USA)
820
821 Results were represented as mean with standard deviation (SD) analyzed by GraphPad Prism.
822 Statistical significance between different biological samples was determined by either paired
823 Student's t test or one-way/ two-way ANOVA with Tukey test for multiple comparisons, if not
824 described otherwise.
825

826 **References**
827

828 1 Kandasamy, P., Gyimesi, G., Kanai, Y. & Hediger, M. A. Amino acid transporters
829 revisited: New views in health and disease. *Trends in biochemical sciences* **43**, 752-
830 789, doi:10.1016/j.tibs.2018.05.003 (2018).
831 2 Chidley, C. *et al.* A CRISPRi/a screening platform to study cellular nutrient transport in
832 diverse microenvironments. *Nat Cell Biol* **26**, 825-838, doi:10.1038/s41556-024-
833 01402-1 (2024).
834 3 White, P. J. *et al.* Insulin action, type 2 diabetes, and branched-chain amino acids: A
835 two-way street. *Mol Metab* **52**, 101261, doi:10.1016/j.molmet.2021.101261 (2021).
836 4 Errasti-Murugarren, E. & Palacin, M. Heteromeric Amino Acid Transporters in Brain:
837 from Physiology to Pathology. *Neurochem Res* **47**, 23-36, doi:10.1007/s11064-021-
838 03261-w (2022).
839 5 Palm, W. & Thompson, C. B. Nutrient acquisition strategies of mammalian cells.
840 *Nature* **546**, 234-242, doi:10.1038/nature22379 (2017).
841 6 Hansen, C. G., Ng, Y. L., Lam, W. L., Plouffe, S. W. & Guan, K. L. The Hippo pathway
842 effectors YAP and TAZ promote cell growth by modulating amino acid signaling to
843 mTORC1. *Cell Res* **25**, 1299-1313, doi:10.1038/cr.2015.140 (2015).
844 7 Hayashi, K., Jutabha, P., Endou, H. & Anzai, N. c-Myc is crucial for the expression of
845 LAT1 in MIA Paca-2 human pancreatic cancer cells. *Oncol Rep* **28**, 862-866,
846 doi:10.3892/or.2012.1878 (2012).
847 8 Kandasamy, P. *et al.* Oncogenic KRAS mutations enhance amino acid uptake by
848 colorectal cancer cells via the hippo signaling effector YAP1. *Mol Oncol*,
849 doi:10.1002/1878-0261.12999 (2021).
850 9 Yue, M., Jiang, J., Gao, P., Liu, H. & Qing, G. Oncogenic MYC Activates a Feedforward
851 Regulatory Loop Promoting Essential Amino Acid Metabolism and Tumorigenesis. *Cell*
852 *Rep* **21**, 3819-3832, doi:10.1016/j.celrep.2017.12.002 (2017).
853 10 Coller, H. A. Cell biology. The essence of quiescence. *Science* **334**, 1074-1075,
854 doi:10.1126/science.1216242 (2011).
855 11 Marescal, O. & Cheeseman, I. M. Cellular Mechanisms and Regulation of Quiescence.
856 *Dev Cell* **55**, 259-271, doi:10.1016/j.devcel.2020.09.029 (2020).
857 12 Rathmell, J. C., Vander Heiden, M. G., Harris, M. H., Frauwirth, K. A. & Thompson, C.
858 B. In the absence of extrinsic signals, nutrient utilization by lymphocytes is
859 insufficient to maintain either cell size or viability. *Mol Cell* **6**, 683-692,
860 doi:10.1016/s1097-2765(00)00066-6 (2000).
861 13 Muller, M. *et al.* The coordinated action of the MVB pathway and autophagy ensures
862 cell survival during starvation. *Elife* **4**, e07736, doi:10.7554/eLife.07736 (2015).
863 14 Patwari, P. & Lee, R. T. An expanded family of arrestins regulate metabolism. *Trends*
864 *Endocrinol Metab* **23**, 216-222, doi:10.1016/j.tem.2012.03.003 (2012).
865 15 Alvarez, C. E. On the origins of arrestin and rhodopsin. *BMC Evol Biol* **8**, 222,
866 doi:10.1186/1471-2148-8-222 (2008).
867 16 Ivashov, V. *et al.* Complementary alpha-arrestin-ubiquitin ligase complexes control
868 nutrient transporter endocytosis in response to amino acids. *Elife* **9**,
869 doi:10.7554/eLife.58246 (2020).
870 17 Lin, C. H., MacGurn, J. A., Chu, T., Stefan, C. J. & Emr, S. D. Arrestin-related ubiquitin-
871 ligase adaptors regulate endocytosis and protein turnover at the cell surface. *Cell*
872 **135**, 714-725 (2008).

873 18 Nikko, E., Sullivan, J. A. & Pelham, H. R. Arrestin-like proteins mediate ubiquitination
874 and endocytosis of the yeast metal transporter Smf1. *EMBO Rep* **9**, 1216-1221,
875 doi:10.1038/embor.2008.199 (2008).
876 19 Liu, Y. *et al.* Structural basis for the regulatory role of the PPxY motifs in the
877 thioredoxin-interacting protein TXNIP. *Biochem J* **473**, 179-187,
878 doi:10.1042/BJ20150830 (2016).
879 20 Nabhan, J. F., Pan, H. & Lu, Q. Arrestin domain-containing protein 3 recruits the
880 NEDD4 E3 ligase to mediate ubiquitination of the beta2-adrenergic receptor. *EMBO*
881 *Rep* **11**, 605-611, doi:embor201080 [pii] 10.1038/embor.2010.80 (2010).
882 21 Rauch, S. & Martin-Serrano, J. Multiple interactions between the ESCRT machinery
883 and arrestin-related proteins: implications for PPXY-dependent budding. *J Virol* **85**,
884 3546-3556, doi:10.1128/JVI.02045-10 JVI.02045-10 [pii] (2011).
885 22 Zhang, P. *et al.* The ubiquitin ligase itch regulates apoptosis by targeting thioredoxin-
886 interacting protein for ubiquitin-dependent degradation. *J Biol Chem* **285**, 8869-8879,
887 doi:10.1074/jbc.M109.063321 (2010).
888 23 Patwari, P., Higgins, L. J., Chutkow, W. A., Yoshioka, J. & Lee, R. T. The interaction of
889 thioredoxin with Txnip. Evidence for formation of a mixed disulfide by disulfide
890 exchange. *J Biol Chem* **281**, 21884-21891, doi:10.1074/jbc.M600427200 (2006).
891 24 Hwang, J. *et al.* The structural basis for the negative regulation of thioredoxin by
892 thioredoxin-interacting protein. *Nat Commun* **5**, 2958, doi:10.1038/ncomms3958
893 (2014).
894 25 Polekhina, G. *et al.* Structure of the N-terminal domain of human thioredoxin-
895 interacting protein. *Acta Crystallogr D Biol Crystallogr* **69**, 333-344,
896 doi:10.1107/S0907444912047099 (2013).
897 26 Waldhart, A. N. *et al.* Phosphorylation of TXNIP by AKT Mediates Acute Influx of
898 Glucose in Response to Insulin. *Cell Rep* **19**, 2005-2013,
899 doi:10.1016/j.celrep.2017.05.041 (2017).
900 27 Wu, N. *et al.* AMPK-dependent degradation of TXNIP upon energy stress leads to
901 enhanced glucose uptake via GLUT1. *Mol Cell* **49**, 1167-1175,
902 doi:10.1016/j.molcel.2013.01.035 (2013).
903 28 Katsu-Jimenez, Y. *et al.* Absence of TXNIP in Humans Leads to Lactic Acidosis and Low
904 Serum Methionine Linked to Deficient Respiration on Pyruvate. *Diabetes* **68**, 709-723,
905 doi:10.2337/db18-0557 (2019).
906 29 Barr, A. R. *et al.* DNA damage during S-phase mediates the proliferation-quiescence
907 decision in the subsequent G1 via p21 expression. *Nat Commun* **8**, 14728,
908 doi:10.1038/ncomms14728 (2017).
909 30 Hinze, C., McGourty, K. & Boucrot, E. Measuring Endocytosis During Proliferative Cell
910 Quiescence. *Methods Mol Biol* **2233**, 19-42, doi:10.1007/978-1-0716-1044-2_2
911 (2021).
912 31 Kirchhausen, T., Macia, E. & Pelish, H. E. Use of dynasore, the small molecule
913 inhibitor of dynamin, in the regulation of endocytosis. *Methods Enzymol* **438**, 77-93,
914 doi:10.1016/S0076-6879(07)38006-3 (2008).
915 32 Macia, E. *et al.* Dynasore, a cell-permeable inhibitor of dynamin. *Dev Cell* **10**, 839-
916 850, doi:10.1016/j.devcel.2006.04.002 (2006).
917 33 Ivashov, V. *et al.* Complementary α-arrestin-ubiquitin ligase complexes control
918 nutrient transporter endocytosis in response to amino acids. *Elife* **9**,
919 doi:10.7554/eLife.58246 (2020).

920 34 Nishinaka, Y. *et al.* Importin alpha1 (Rch1) mediates nuclear translocation of
921 thioredoxin-binding protein-2/vitamin D(3)-up-regulated protein 1. *J Biol Chem* **279**,
922 37559-37565, doi:10.1074/jbc.M405473200 (2004).
923 35 Saxena, G., Chen, J. & Shalev, A. Intracellular shuttling and mitochondrial function of
924 thioredoxin-interacting protein. *J Biol Chem* **285**, 3997-4005,
925 doi:10.1074/jbc.M109.034421 (2010).
926 36 Qualls-Histed, S. J., Nielsen, C. P. & MacGurn, J. A. Lysosomal trafficking of the
927 glucose transporter GLUT1 requires sequential regulation by TXNIP and ubiquitin.
928 *iScience* **26**, 106150, doi:10.1016/j.isci.2023.106150 (2023).
929 37 Kim, S. *et al.* TXNIP-mediated crosstalk between oxidative stress and glucose
930 metabolism. *PLoS One* **19**, e0292655, doi:10.1371/journal.pone.0292655 (2024).
931 38 Hytti, M. *et al.* Phloretin inhibits glucose transport and reduces inflammation in
932 human retinal pigment epithelial cells. *Mol Cell Biochem* **478**, 215-227,
933 doi:10.1007/s11010-022-04504-2 (2023).
934 39 Qi, S., O'Hayre, M., Gutkind, J. S. & Hurley, J. H. Structural and biochemical basis for
935 ubiquitin ligase recruitment by arrestin-related domain-containing protein-3
936 (ARRDC3). *J Biol Chem* **289**, 4743-4752, doi:10.1074/jbc.M113.527473 (2014).
937 40 Shea, F. F., Rowell, J. L., Li, Y., Chang, T. H. & Alvarez, C. E. Mammalian alpha arrestins
938 link activated seven transmembrane receptors to Nedd4 family e3 ubiquitin ligases
939 and interact with beta arrestins. *PLoS One* **7**, e50557,
940 doi:10.1371/journal.pone.0050557 (2012).
941 41 Woelk, T. *et al.* Molecular mechanisms of coupled monoubiquitination. *Nat Cell Biol*
942 **8**, 1246-1254, doi:10.1038/ncb1484 (2006).
943 42 Gahlot, P. *et al.* Lysosomal damage sensing and lysophagy initiation by SPG20-ITCH.
944 *Mol Cell* **84**, 1556-1569 e1510, doi:10.1016/j.molcel.2024.02.029 (2024).
945 43 Patwari, P. *et al.* Thioredoxin-independent regulation of metabolism by the alpha-
946 arrestin proteins. *J Biol Chem* **284**, 24996-25003, doi:10.1074/jbc.M109.018093
947 (2009).
948 44 Oda, K. *et al.* L-type amino acid transporter 1 inhibitors inhibit tumor cell growth.
949 *Cancer Sci* **101**, 173-179, doi:10.1111/j.1349-7006.2009.01386.x (2010).
950 45 Stacpoole, P. W. Therapeutic Targeting of the Pyruvate Dehydrogenase
951 Complex/Pyruvate Dehydrogenase Kinase (PDC/PDK) Axis in Cancer. *J Natl Cancer*
952 *Inst* **109**, doi:10.1093/jnci/djx071 (2017).
953 46 Whitehouse, S., Cooper, R. H. & Randle, P. J. Mechanism of activation of pyruvate
954 dehydrogenase by dichloroacetate and other halogenated carboxylic acids. *Biochem J*
955 **141**, 761-774, doi:10.1042/bj1410761 (1974).
956 47 Knaus, L. S. *et al.* Large neutral amino acid levels tune perinatal neuronal excitability
957 and survival. *Cell* **186**, 1950-1967 e1925, doi:10.1016/j.cell.2023.02.037 (2023).
958 48 Tarlungeanu, D. C. *et al.* Impaired Amino Acid Transport at the Blood Brain Barrier Is
959 a Cause of Autism Spectrum Disorder. *Cell* **167**, 1481-1494 e1418,
960 doi:10.1016/j.cell.2016.11.013 (2016).
961 49 Hui, S. T. *et al.* Txnip balances metabolic and growth signaling via PTEN disulfide
962 reduction. *Proc Natl Acad Sci U S A* **105**, 3921-3926, doi:10.1073/pnas.0800293105
963 (2008).
964 50 Hui, T. Y. *et al.* Mice lacking thioredoxin-interacting protein provide evidence linking
965 cellular redox state to appropriate response to nutritional signals. *J Biol Chem* **279**,
966 24387-24393, doi:10.1074/jbc.M401280200 (2004).

967 51 Sheth, S. S. *et al.* Thioredoxin-interacting protein deficiency disrupts the fasting-
968 feeding metabolic transition. *J Lipid Res* **46**, 123-134, doi:10.1194/jlr.M400341-
969 JLR200 (2005).
970 52 Chutkow, W. A., Patwari, P., Yoshioka, J. & Lee, R. T. Thioredoxin-interacting protein
971 (Txnip) is a critical regulator of hepatic glucose production. *J Biol Chem* **283**, 2397-
972 2406, doi:10.1074/jbc.M708169200 (2008).
973 53 Coloff, J. L. *et al.* Differential Glutamate Metabolism in Proliferating and Quiescent
974 Mammary Epithelial Cells. *Cell Metab* **23**, 867-880, doi:10.1016/j.cmet.2016.03.016
975 (2016).
976 54 Edinger, A. L. & Thompson, C. B. Akt maintains cell size and survival by increasing
977 mTOR-dependent nutrient uptake. *Mol Biol Cell* **13**, 2276-2288, doi:10.1091/mbc.01-
978 12-0584 (2002).
979 55 Lee, H. J. *et al.* Proteomic and Metabolomic Characterization of a Mammalian Cellular
980 Transition from Quiescence to Proliferation. *Cell Rep* **20**, 721-736,
981 doi:10.1016/j.celrep.2017.06.074 (2017).
982 56 Kanai, Y. Amino acid transporter LAT1 (SLC7A5) as a molecular target for cancer
983 diagnosis and therapeutics. *Pharmacol Ther* **230**, 107964,
984 doi:10.1016/j.pharmthera.2021.107964 (2022).
985 57 Kaira, K. *et al.* Clinical significance of L-type amino acid transporter 1 expression as a
986 prognostic marker and potential of new targeting therapy in biliary tract cancer. *BMC*
987 *Cancer* **13**, 482, doi:10.1186/1471-2407-13-482 (2013).
988 58 Kalaany, N. How nearby nutrients shape tumor growth. *Elife* **12**,
989 doi:10.7554/eLife.89825 (2023).
990 59 Barthelemy, C. & Andre, B. Ubiquitylation and endocytosis of the human
991 LAT1/SLC7A5 amino acid transporter. *Sci Rep* **9**, 16760, doi:10.1038/s41598-019-
992 53065-w (2019).
993 60 Rosario, F. J., Dimasuay, K. G., Kanai, Y., Powell, T. L. & Jansson, T. Regulation of
994 amino acid transporter trafficking by mTORC1 in primary human trophoblast cells is
995 mediated by the ubiquitin ligase Nedd4-2. *Clin Sci (Lond)* **130**, 499-512,
996 doi:10.1042/CS20150554 (2016).
997 61 Teis, D. *et al.* p14-MP1-MEK1 signaling regulates endosomal traffic and cellular
998 proliferation during tissue homeostasis. *J Cell Biol* **175**, 861-868, doi:jcb.200607025
999 [pii] 10.1083/jcb.200607025 (2006).
1000 62 Cormerais, Y. *et al.* The glutamine transporter ASCT2 (SLC1A5) promotes tumor
1001 growth independently of the amino acid transporter LAT1 (SLC7A5). *J Biol Chem* **293**,
1002 2877-2887, doi:10.1074/jbc.RA117.001342 (2018).
1003 63 Schmidt, O. *et al.* Endosome and Golgi-associated degradation (EGAD) of membrane
1004 proteins regulates sphingolipid metabolism. *EMBO J* **38**, e101433,
1005 doi:10.15252/embj.2018101433 (2019).
1006 64 Ran, F. A. *et al.* Genome engineering using the CRISPR-Cas9 system. *Nat Protoc* **8**,
1007 2281-2308, doi:10.1038/nprot.2013.143 (2013).
1008 65 Finicle, B. T. *et al.* Sphingolipids inhibit endosomal recycling of nutrient transporters
1009 by inactivating ARF6. *J Cell Sci* **131**, doi:10.1242/jcs.213314 (2018).
1010 66 Zou, C., Wang, Y. & Shen, Z. 2-NBDG as a fluorescent indicator for direct glucose
1011 uptake measurement. *J Biochem Biophys Methods* **64**, 207-215,
1012 doi:10.1016/j.jbbm.2005.08.001 (2005).

1013 67 van Pijkeren, A. *et al.* Proteome Coverage after Simultaneous Proteo-Metabolome
1014 Liquid-Liquid Extraction. *J Proteome Res* **22**, 951-966,
1015 doi:10.1021/acs.jproteome.2c00758 (2023).
1016 68 Kipura, T. *et al.* Automated Liquid Handling Extraction and Rapid Quantification of
1017 Underivatized Amino Acids and Tryptophan Metabolites from Human Serum and
1018 Plasma Using Dual-Column U(H)PLC-MRM-MS and Its Application to Prostate Cancer
1019 Study. *Metabolites* **14**, doi:10.3390/metabo14070370 (2024).
1020

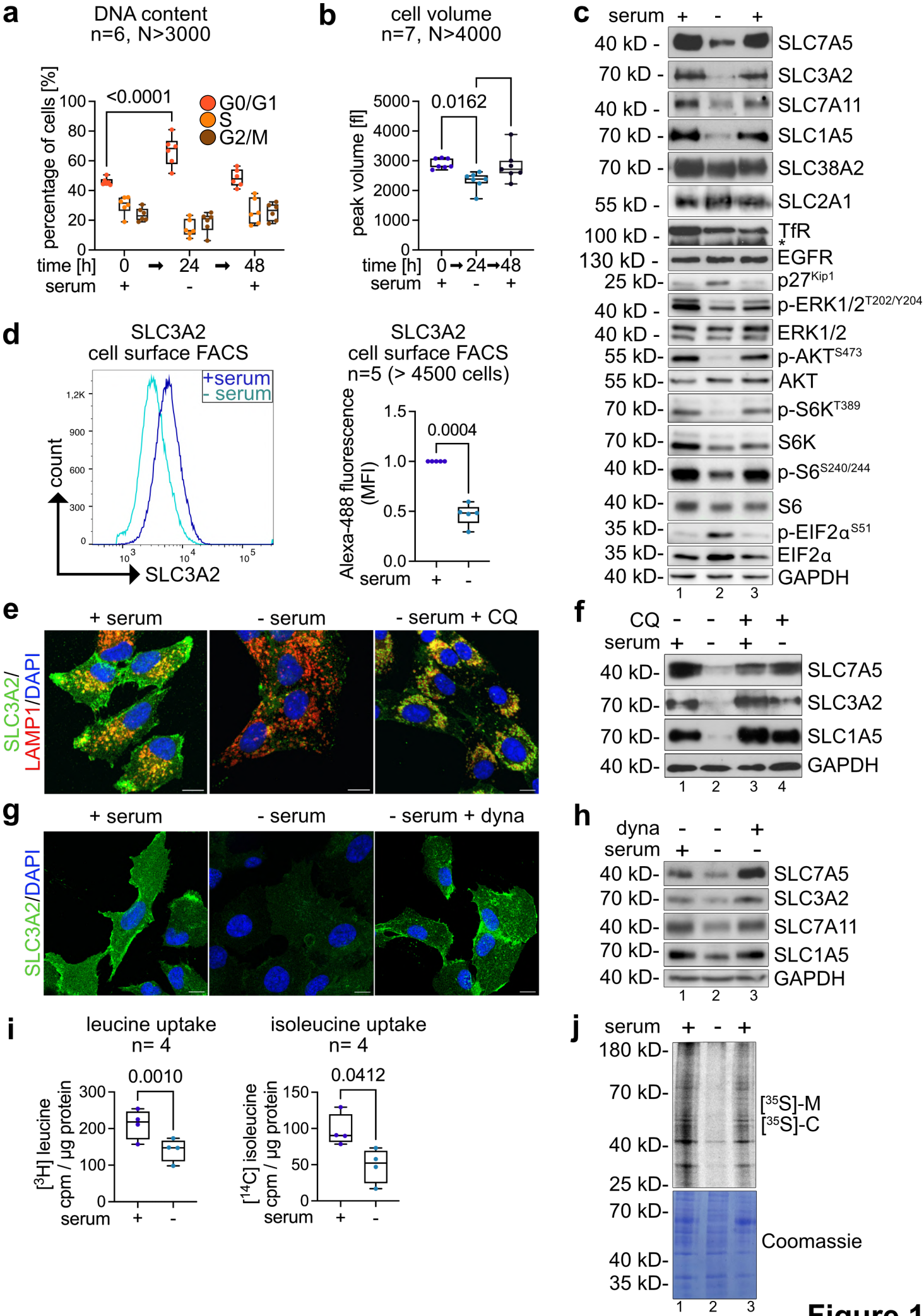
a
DNA content
n=6, N>3000
percentage of cells [%]
<0.0001
G0/G1
S
G2/M
time [h] 0 → 24 → 48
serum + - +
b
cell volume
n=7, N>4000
peak volume [fl]
0.0162
time [h] 0 → 24 → 48
serum + - +
c
serum + - +
40 kD - SLC7A5
70 kD - SLC3A2
40 kD - SLC7A11
70 kD - SLC1A5
70 kD - SLC38A2
55 kD - SLC2A1
100 kD - TfR
130 kD - * EGFR
25 kD- p27Kip1
40 kD - p-ERK1/2T202/Y204
40 kD - ERK1/2
55 kD- p-AKTS473
55 kD- AKT
70 kD- p-S6KT389
70 kD- S6K
40 kD- p-S6S240/244
40 kD- S6
35 kD- p-EIF2αS51
35 kD- EIF2α
40 kD- GAPDH
1 2 3
d
SLC3A2
cell surface FACS
+serum
- serum
count
SLC3A2
SLC3A2
cell surface FACS
n=5 (> 4500 cells)
Alexa-488 fluorescence (MFI)
0.0004
serum + -
e
+ serum
- serum
- serum + CQ
SLC3A2/
LAMP1/DAPI
f
CQ - - + +
serum + - + -
40 kD- SLC7A5
70 kD- SLC3A2
70 kD- SLC1A5
40 kD- GAPDH
1 2 3 4
g
+ serum
- serum
- serum + dyna
SLC3A2/DAPI
h
dyna - - +
serum + - -
40 kD- SLC7A5
70 kD- SLC3A2
40 kD- SLC7A11
70 kD- SLC1A5
40 kD- GAPDH
1 2 3
i
leucine uptake
n= 4
[3H] leucine cpm / µg protein
0.0010
serum + -
isoleucine uptake
n= 4
[14C] isoleucine cpm / µg protein
0.0412
serum + -
j
serum + - +
180 kD-
70 kD-
40 kD-
25 kD-
[35S]-M
[35S]-C
70 kD-
40 kD-
35 kD-
Coomassie
1 2 3

Figure 1

Figure 1. Dynamin-dependent endocytosis and lysosomal degradation of SLC7A5 and SLC1A5.

RPE1 cells were grown in DMEM supplemented with serum (0 h, + serum), cultured in serum free medium for 24 h (24 h, - serum) and refed with serum for 24 h (48 h, + serum). **(a)** Cells were harvested, permeabilized and fixed, and the DNA content was analyzed by propidium iodide (PI) staining to assess the cell cycle profile by FACS (n=6, N>3000 cells, two-way ANOVA, Tukey's multiple comparisons test). **(b)** Peak volume (in fl) was assessed by CASY Cell Counter and Analyzer (n=7, N>4000 cells, one-way ANOVA, Tukey's multiple comparisons test). **(c)** Total cells lysates were analyzed by SDS-PAGE and Western Blot (WB) with the indicated antibodies. **(d)** The cell surface was stained with anti-SLC3A2 and anti-mouse Alexa-488. FACS was used to detect SLC3A2 surface staining. A representative histogram is shown. Quantification of the fluorescence intensities of SLC3A2 was normalized to proliferating cells (+ serum) (n=5, N>4500 cells, paired t-test). **(e, g)** Indirect immunofluorescence (IF) of PFA fixed cells stained for SLC3A2 (green), LAMP1 (red) and DAPI (blue) were analyzed by confocal microscopy. The merged images show a single plane of a Z-stack. Scale bar = 10 µm. **(e)** Incubation with 12.5 µM chloroquine (CQ) in absence of serum for 14 h (- serum, + CQ). **(g)** Incubation with 20 µM dynasore (dyna) in absence of serum for 14 h (- serum, + dyna). **(f, h)** Total cells lysates of cells treated as in (e, g) were analyzed by SDS-PAGE and WB with the indicated antibodies. **(i)** Cells were incubated with [^{3}H]-leucine or [^{14}C]-isoleucine for 15 min, washed and lysed. Total cell lysates were analyzed by scintillation counting. Counts per minute (cpm) values were normalized to total protein content (cpm / µg protein, n=4, paired t-test). **(j)** Cells were incubated with [^{35}S]-methionine, [^{35}S]-cysteine for 2 minutes, before cycloheximide (CHX, 10 µg/ml) was added, cells were lysed and analyzed by SDS-PAGE and autoradiography.

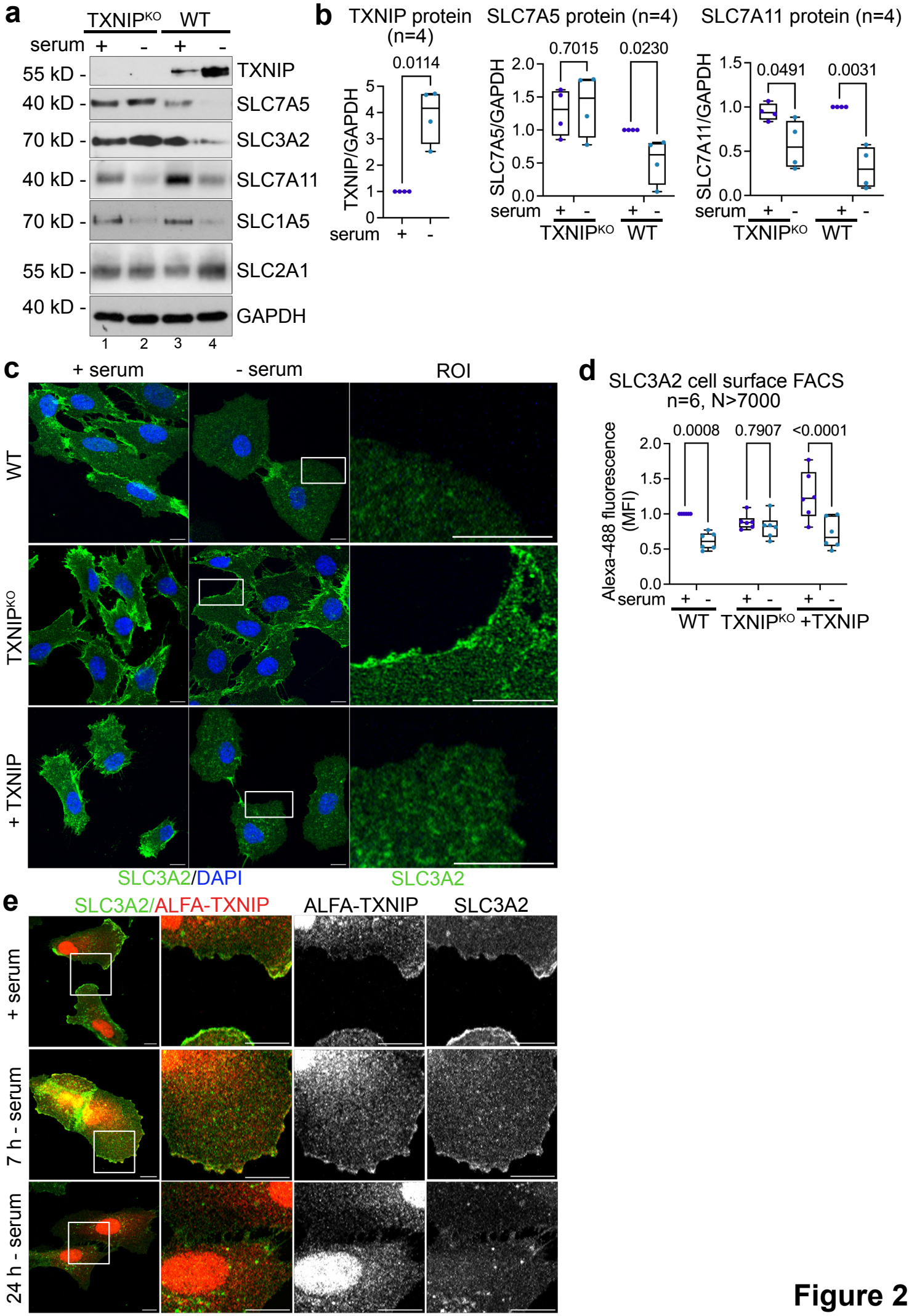
a
TXNIPKO
WT
serum + - + -
55 kD -
40 kD -
70 kD -
40 kD -
70 kD -
55 kD -
40 kD -
TXNIP
SLC7A5
SLC3A2
SLC7A11
SLC1A5
SLC2A1
GAPDH
1 2 3 4
b
TXNIP protein (n=4)
0.0114
TXNIP/GAPDH
serum + -
SLC7A5 protein (n=4)
0.7015
0.0230
SLC7A5/GAPDH
serum + - + -
TXNIPKO WT
SLC7A11 protein (n=4)
0.0491
0.0031
SLC7A11/GAPDH
serum + - + -
TXNIPKO WT
c
+ serum
- serum
ROI
WT
TXNIPKO
+ TXNIP
SLC3A2/DAPI
SLC3A2
d
SLC3A2 cell surface FACS
n=6, N>7000
0.0008
0.7907
<0.0001
Alexa-488 fluorescence (MFI)
serum + - + - + -
WT TXNIPKO +TXNIP
e
SLC3A2/ALFA-TXNIP
ALFA-TXNIP
SLC3A2
+ serum
7 h - serum
24 h - serum

Figure 2

Figure 2. The importance of TXNIP for the selective degradation of SLC7A5.

(a) $TXNIP^{KO}$ and WT cells were grown in growth medium (+ serum) or serum starved for 24 h (- serum). Total cell lysates were analyzed by SDS-PAGE and WB with the indicated antibodies. **(b)** WB quantification of TXNIP (n=4, paired t-test), SLC7A5 (n=4, two-way ANOVA, Sidak's multiple comparisons test) and SLC7A11 protein levels (n=4, two-way ANOVA, Sidak's multiple comparisons test). Values were normalized to proliferating WT cells (+ serum). **(c)** IF of PFA fixed cells (WT, $TXNIP^{KO}$ and $TXNIP^{KO}$ reconstituted with TXNIP) stained for SLC3A2 (green) and DAPI (blue) were analyzed by confocal microscopy. The images show a single plane of a Z-stack. Regions of interest (ROI, white box) were magnified. Scale bar = 10 µm. **(d)** Quantification of SLC3A2 cell surface FACS of the indicated cells, normalized to proliferating WT cells (n=6, N>7000, two-way ANOVA, Sidak's multiple comparisons test). **(e)** IF of PFA fixed $TXNIP^{KO}$ reconstituted with ALFA-TXNIP. The localization of ALFA-TXNIP (red) and SLC3A2 (green) was analyzed by confocal microscopy. The images show a single plane of a Z-stack. Regions of interest (ROI, white box) were magnified. Scale bar = 10 µm.

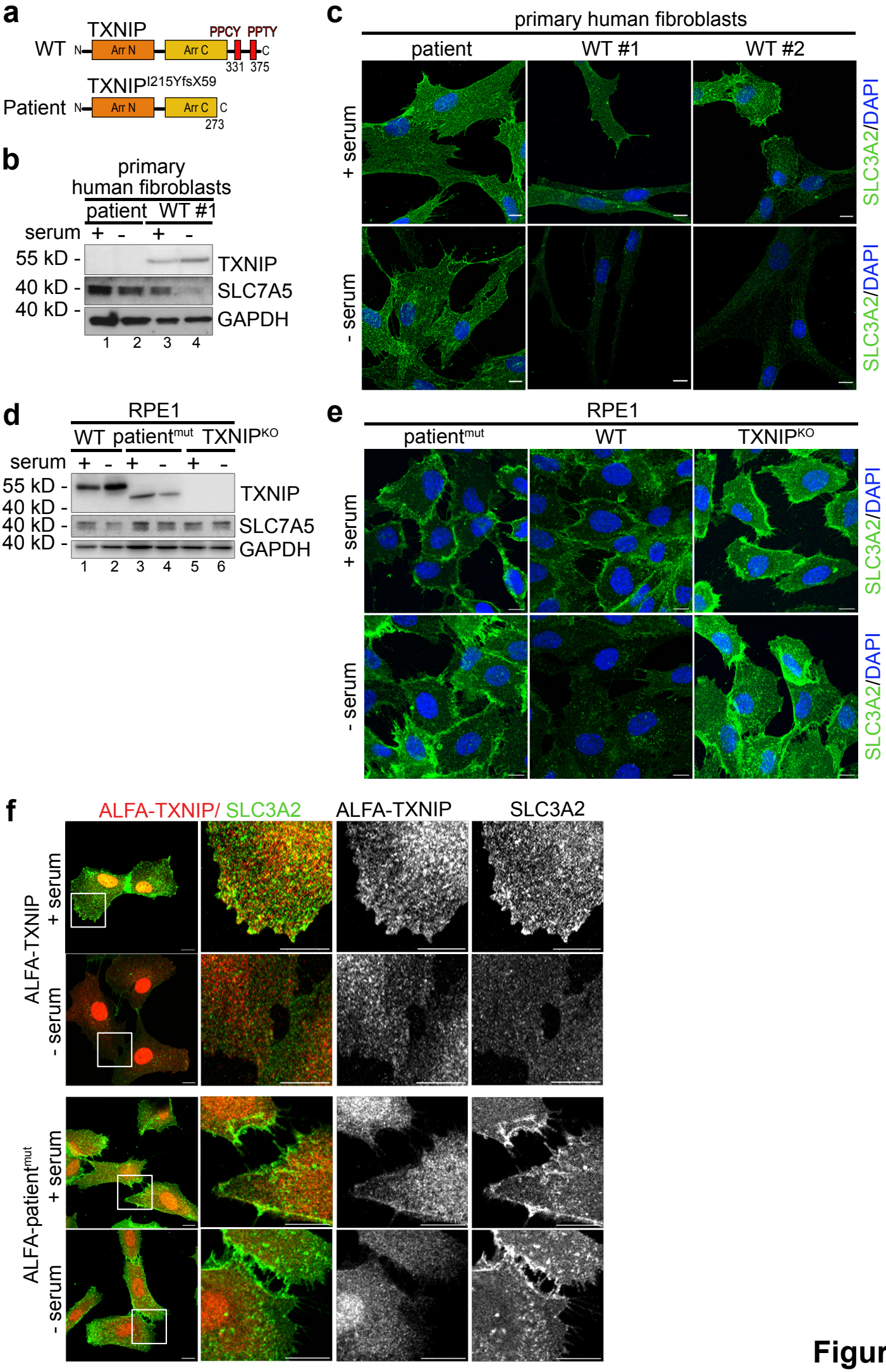
a
TXNIP
WT
N
Arr N
Arr C
PPCY PPTY
C
331 375
TXNIP I215YfsX59
Patient
N
Arr N
Arr C
C
273
b
primary human fibroblasts
patient WT #1
serum + - + -
55 kD -
40 kD -
40 kD -
TXNIP
SLC7A5
GAPDH
1 2 3 4
c
primary human fibroblasts
patient
WT #1
WT #2
+ serum
- serum
SLC3A2/DAPI
SLC3A2/DAPI
d
RPE1
WT patient mut TXNIP KO
serum + - + - + -
55 kD -
40 kD -
40 kD -
40 kD -
TXNIP
SLC7A5
GAPDH
1 2 3 4 5 6
e
RPE1
patient mut
WT
TXNIP KO
+ serum
- serum
SLC3A2/DAPI
SLC3A2/DAPI
f
ALFA-TXNIP/ SLC3A2
ALFA-TXNIP
SLC3A2
ALFA-TXNIP
+ serum
- serum
ALFA-patient mut
+ serum
- serum

Figure 3

Figure 3. Loss of function mutation in TXNIP causes a rare disease.

(a) Schematic representation of WT TXNIP and mutant TXNIP harboring the patient mutation (c.642_643insT, patient^{mut}). **(b, c)** Control fibroblasts (WT#1 and WT#2) and patient-derived fibroblasts (patient) were grown in growth medium (+ serum) or serum starved for 24 h (- serum). **(b)** Total cell lysates were analyzed by SDS-PAGE and WB with the indicated antibodies. **(c)** Indirect IF of PFA fixed fibroblasts (patient, WT#1, WT#2) stained for SLC3A2 (green) and DAPI (blue) was analyzed by confocal microscopy. The images show a single plane of a Z-stack. Scale bar = 10 µm. (**d, e)** RPE1 WT, TXNIP^{KO} and TXNIP^{KO} reconstituted with ALFA-TXNIP harboring the patient mutation (c.642_643insT, patient^{mut}) were grown in growth medium (+ serum) or serum starved for 24 h (- serum). **(d)** Total cell lysates were analyzed by SDS-PAGE and WB with the indicated antibodies. **(e)** Indirect IF of PFA fixed cells (WT, TXNIP^{KO} and patient^{mut}) stained for SLC3A2 (green) and DAPI (blue) was analyzed by confocal microscopy. The images show a single plane of a Z-stack. Scale bar = 10 µm. **(f)** ALFA-TXNIP (red) and SLC3A2 (green) was analyzed by confocal microscopy. The images show a single plane of a Z-stack. Regions of interest (ROI, white box) were magnified. Scale bar = 10 µm.

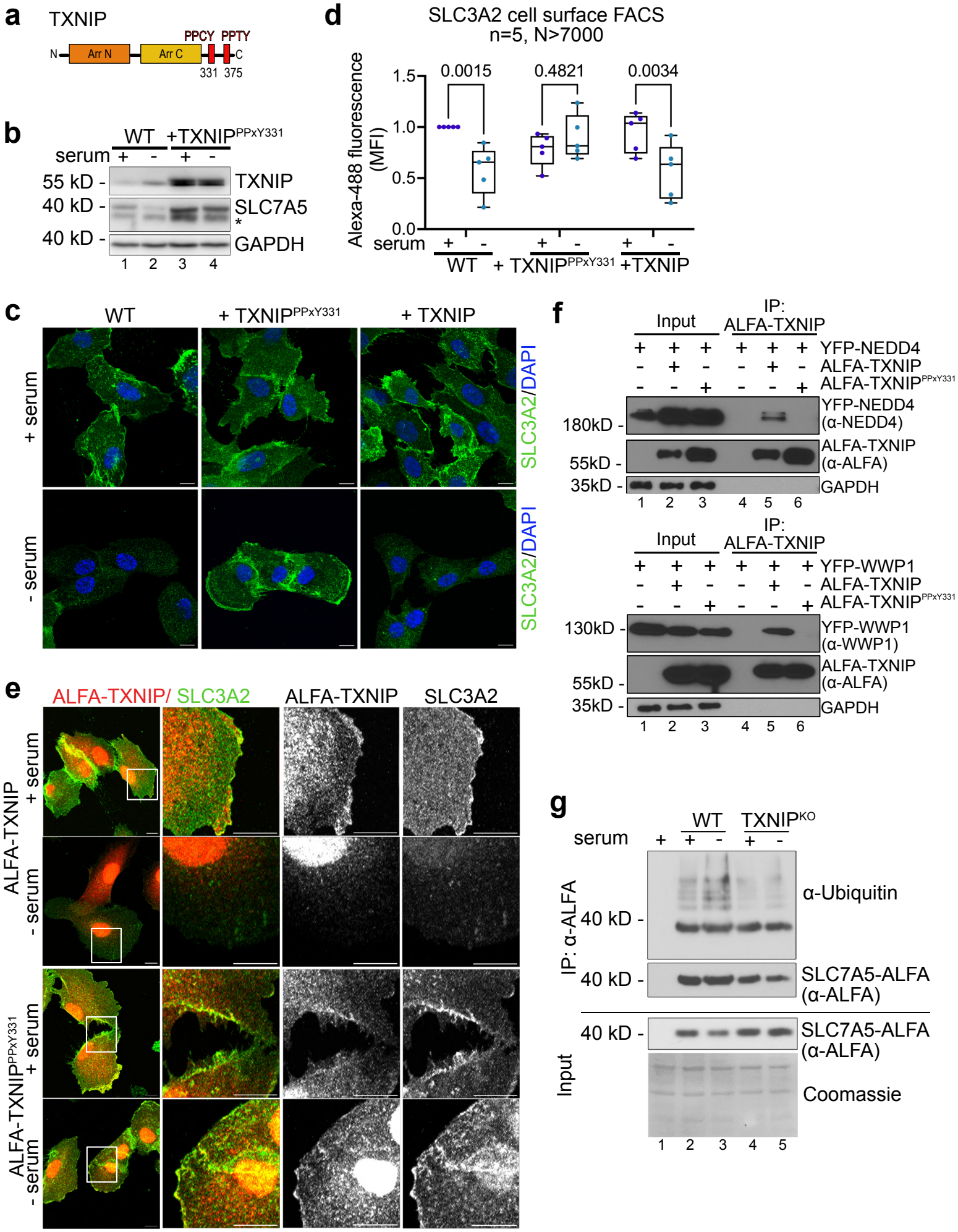
a
TXNIP
PPCY PPTY
N
Arr N
Arr C
C
331 375
b
WT +TXNIP PPxY331
serum + - + -
55 kD -
40 kD -
40 kD -
TXNIP
SLC7A5
*
GAPDH
1 2 3 4
d
SLC3A2 cell surface FACS
n=5, N>7000
Alexa-488 fluorescence (MFI)
1.5
1.0
0.5
0.0
0.0015
0.4821
0.0034
serum + - + - + -
WT + TXNIP PPxY331 +TXNIP
c
WT
+ TXNIP PPxY331
+ TXNIP
+ serum
- serum
SLC3A2/DAPI
SLC3A2/DAPI
e
ALFA-TXNIP/ SLC3A2
ALFA-TXNIP
SLC3A2
ALFA-TXNIP
+ serum
- serum
ALFA-TXNIP PPxY331
+ serum
- serum
f
Input
IP: ALFA-TXNIP
+ + + + + + YFP-NEDD4
- + - - + - ALFA-TXNIP
- - + - - + ALFA-TXNIP PPxY331
180kD -
55kD -
35kD -
YFP-NEDD4 (α-NEDD4)
ALFA-TXNIP (α-ALFA)
GAPDH
1 2 3 4 5 6
Input
IP: ALFA-TXNIP
+ + + + + + YFP-WWP1
- + - - + - ALFA-TXNIP
- - + - - + ALFA-TXNIP PPxY331
130kD -
55kD -
35kD -
YFP-WWP1 (α-WWP1)
ALFA-TXNIP (α-ALFA)
GAPDH
1 2 3 4 5 6
g
serum + + - + -
WT
TXNIP KO
IP: α-ALFA
40 kD -
40 kD -
α-Ubiquitin
SLC7A5-ALFA (α-ALFA)
Input
40 kD -
SLC7A5-ALFA (α-ALFA)
Coomassie
1 2 3 4 5

Figure 4

Figure 4. PPxY motifs of TXNIP in the downregulation of SLC7A5.

(a) Schematic representation of TXNIP protein harboring PPxY motifs. **(b)** Total cell lysates from WT cells or TXNIP^{KO} reconstituted with ALFA-TXNIP^{PPxY331} mutants were analyzed by SDS-PAGE and WB with the indicated antibodies. The asterisk (*) labels a second band that was only detected using the monoclonal SLC7A5 antibody. **(c, e)** Indirect IF of PFA fixed cells (WT, TXNIP^{KO} and TXNIP^{KO} reconstituted with ALFA-TXNIP or ALFA-TXNIP^{PPXY331}) was analyzed by confocal microscopy. The images show a single plane of a Z-stack **(c)** Cells were stained for SLC3A2 (green) and DAPI (blue). Scale bar = 10 µm. **(d)** Quantification of SLC3A2 cell surface FACS of the indicated cells, normalized to proliferating WT cells (n=5, N>7000 cells, two-way ANOVA, Sidak's multiple comparisons test). **(e)** Cells were stained for ALFA-TXNIP (red) and SLC3A2 (green). Regions of interest (ROI, white box) were magnified. Scale bar = 10 µm**.** **(f)** SDS-PAGE and WB analysis with the indicated antibodies from non-denaturing ALFA-immunoprecipitations (IP) from HEK293T cells expressing ALFA-TXNIP or the mutated ALFA-TXNIP^{PPxY331} variant and the indicated YFP-tagged HECT-type ubiquitin ligase. **(g)** SDS-PAGE and WB analysis with the indicated antibodies from denaturing ALFA-SLC7A5 IP from SLC7A5^{KO} RPE1 reconstituted with ALFA-SLC7A5.

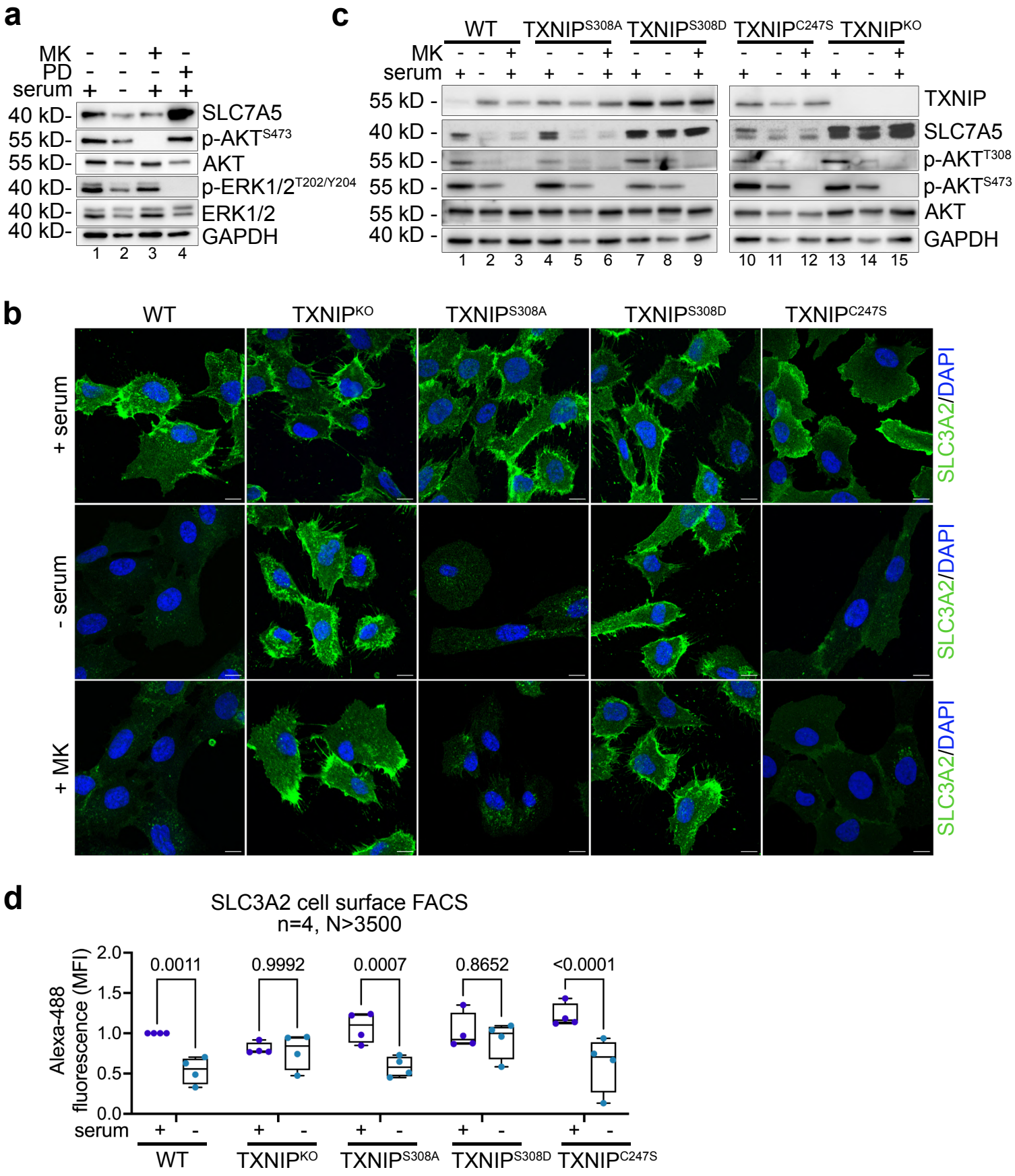
a
MK - - + -
PD - - - +
serum + - + +
40 kD- SLC7A5
55 kD- p-AKT S473
55 kD- AKT
40 kD- p-ERK1/2 T202/Y204
40 kD- ERK1/2
40 kD- GAPDH
1 2 3 4
c
WT TXNIP S308A TXNIP S308D TXNIP C247S TXNIP KO
MK - - + - - + - - + - - + - - +
serum + - + + - + + - + + - + + - +
55 kD - TXNIP
40 kD - SLC7A5
55 kD - p-AKT T308
55 kD - p-AKT S473
55 kD - AKT
40 kD - GAPDH
1 2 3 4 5 6 7 8 9 10 11 12 13 14 15
b
WT
TXNIP KO
TXNIP S308A
TXNIP S308D
TXNIP C247S
+ serum
- serum
+ MK
SLC3A2/DAPI
d
SLC3A2 cell surface FACS
n=4, N>3500
Alexa-488 fluorescence (MFI)
2.0
1.5
1.0
0.5
0.0
0.0011
0.9992
0.0007
0.8652
<0.0001
serum + -
WT
TXNIP KO
TXNIP S308A
TXNIP S308D
TXNIP C247S

Figure 5

Figure 5. TXNIP and AKT signaling.

(a) Total cell lysates from WT cells before or after 24 h of serum starvation or incubation with 1 µM MK2206 (MK) or 5 µM PD0325901 (PD). Cells were analyzed by SDS-PAGE and WB with the indicated antibodies. **(b)** Indirect IF of PFA fixed cells (WT, $TXNIP^{KO}$ and $TXNIP^{KO}$ reconstituted with $TXNIP^{S308A}$, $TXNIP^{S308D}$ or $TXNIP^{C247S}$) before or after serum starvation or incubation with 1 µM MK2206 (MK) stained for SLC3A2 (green) and DAPI (blue). Cells were analyzed by confocal microscopy. The images show a single plane of a Z-stack. Scale bar = 10 µm. **(c)** Total cell lysates from cells treated as in (b) were analyzed by SDS-PAGE and WB with the indicated antibodies. **(d)** Quantification of SLC3A2 cell surface FACS from the indicated cells (n=4, N>3500 cells, two-way ANOVA, Sidak's multiple comparisons test).

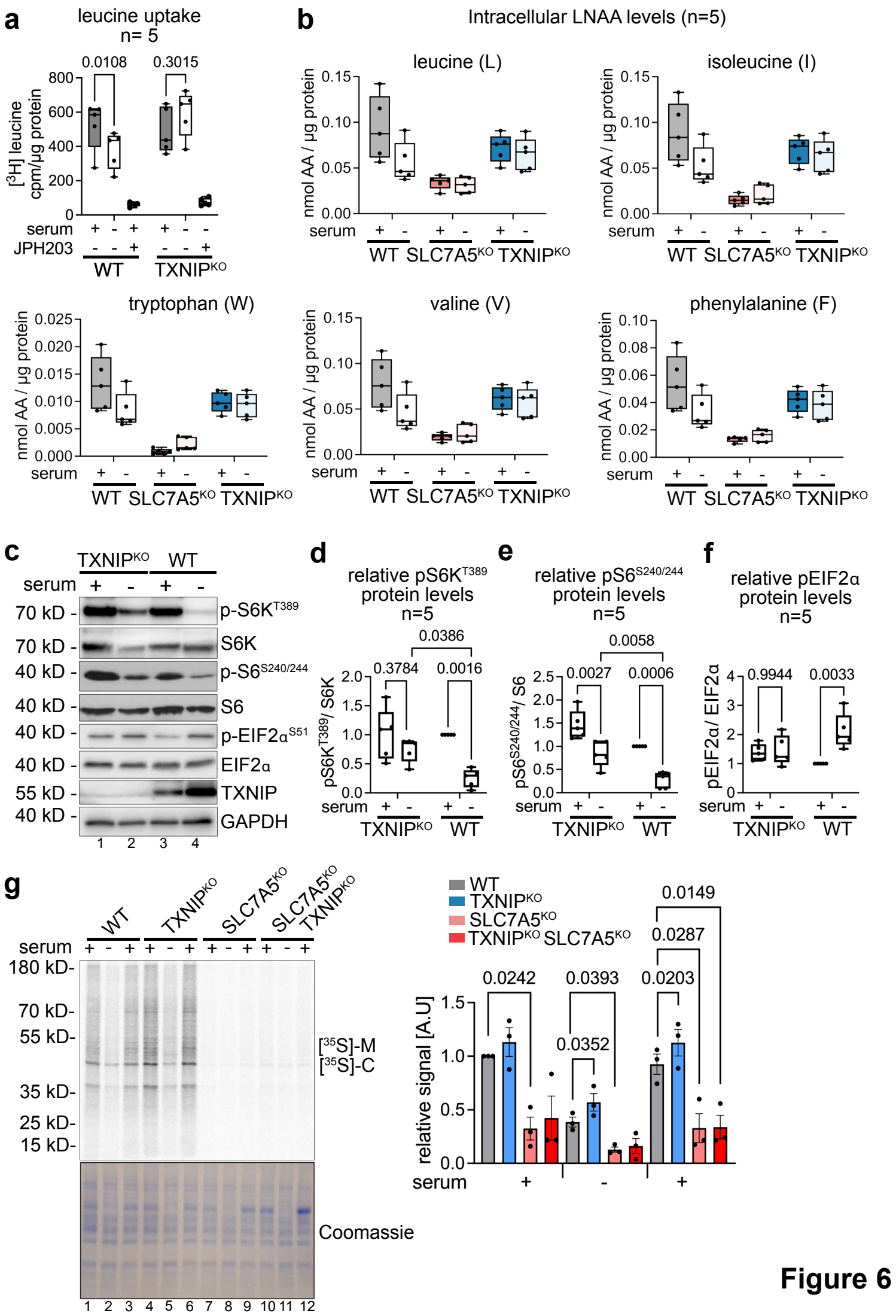
a
leucine uptake
n= 5
0.0108
0.3015
[3H] leucine cpm/µg protein
serum
JPH203
WT
TXNIPKO
b
Intracellular LNAA levels (n=5)
leucine (L)
isoleucine (I)
tryptophan (W)
valine (V)
phenylalanine (F)
nmol AA / µg protein
serum
WT SLC7A5KO TXNIPKO
c
TXNIPKO WT
serum
70 kD - p-S6KT389
70 kD - S6K
40 kD - p-S6S240/244
40 kD - S6
40 kD - p-EIF2αS51
40 kD - EIF2α
55 kD - TXNIP
40 kD - GAPDH
1 2 3 4
d
relative pS6KT389 protein levels n=5
0.0386
0.3784
0.0016
pS6KT389/ S6K
TXNIPKO WT
e
relative pS6S240/244 protein levels n=5
0.0058
0.0027
0.0006
pS6S240/244/ S6
f
relative pEIF2α protein levels n=5
0.9944
0.0033
pEIF2α/ EIF2α
g
WT
TXNIPKO
SLC7A5KO
SLC7A5KO TXNIPKO
180 kD-
70 kD-
55 kD-
35 kD-
25 kD-
15 kD-
[35S]-M
[35S]-C
Coomassie
1 2 3 4 5 6 7 8 9 10 11 12
WT
TXNIPKO
SLC7A5KO
TXNIPKO SLC7A5KO
0.0149
0.0287
0.0242
0.0393
0.0203
0.0352
relative signal [A.U]

Figure 6

Figure 6. TXNIP mediated degradation of SLC7A5 contributed to metabolic signaling

(a) WT and TXNIP^{KO} cells were grown in growth medium (+ serum), serum starved for 24 h (- serum) or treated with 10 μM JPH203. Cells were incubated with [^{3}H]-leucine for 15 min, washed and lysed. Cell lysates were analyzed by scintillation counting. Cpm values were normalized to total protein content (n=5, two-way ANOVA, Tukey's multiple comparisons test). **(b)** WT, SLC7A5^{KO} and TXNIP^{KO} cells were grown in growth medium (+ serum) or serum starved for 24 h (- serum). Mass spectrometry analysis of free AAs, normalized to total protein content (nmol AA / μg protein, n=5). **(c)** Total cell lysates from WT and TXNIP^{KO} cells before or after 24h serum starvation, were analyzed by SDS-PAGE and WB with the indicated antibodies **(d-f)** WB quantification of pS6K^{T389}, normalized to total S6K. WB quantification of pS6$^{S240/244}$, normalized to total S6 and WB quantification of pEIF2α^{S51}, normalized to total EIF2α protein levels (n=5, two-way ANOVA). **(g)** Cells were incubated with [^{35}S]-methionine, [^{35}S]-cysteine for 2 minutes, before CHX (10μg/ml) was added, cells were lysed and analyzed by SDS-PAGE and autoradiography follow by densitometric analysis (n=3, paired t-test).

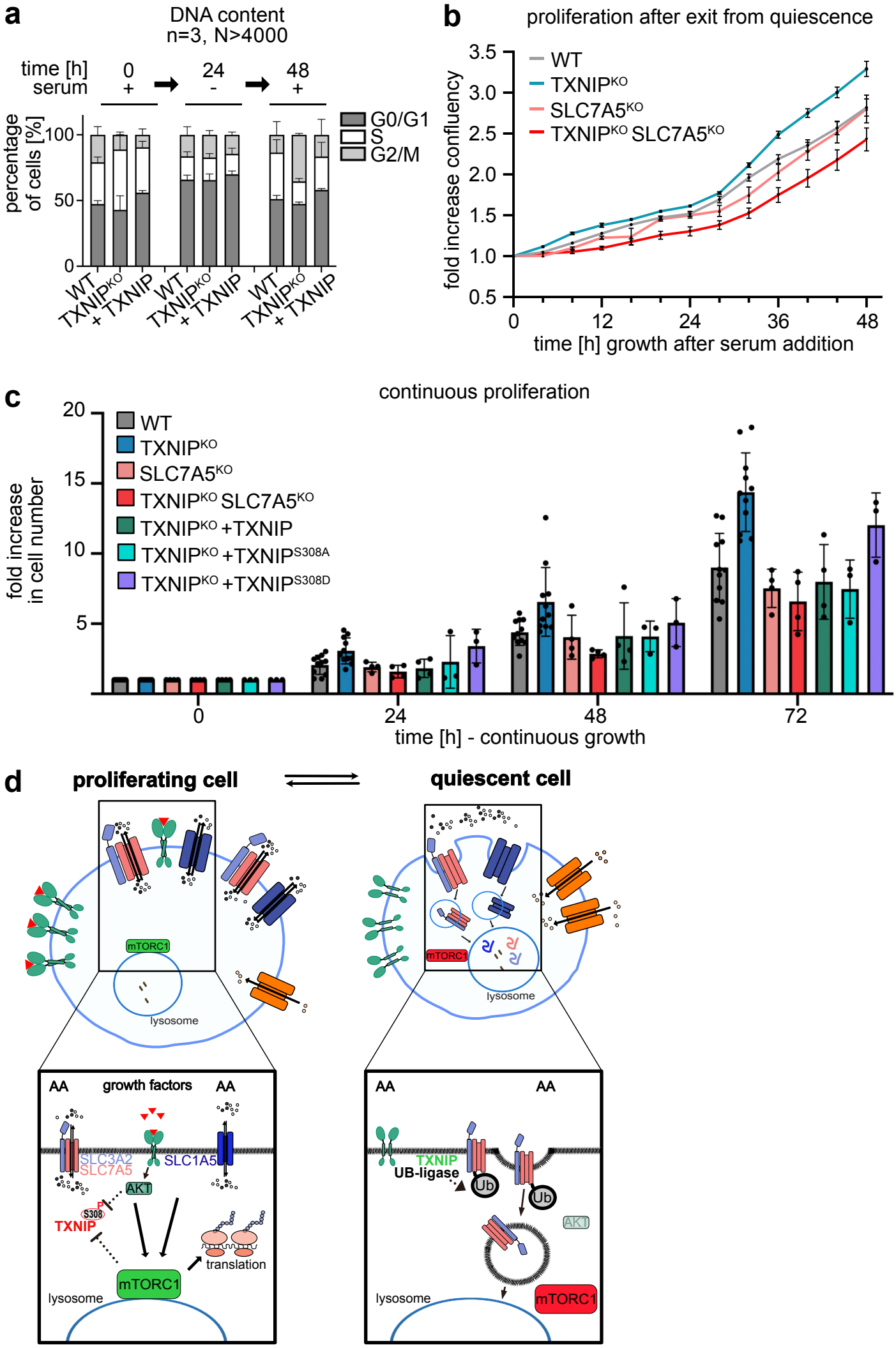
a
DNA content
n=3, N>4000
time [h]
serum
0
+
24
-
48
+
percentage of cells [%]
100
50
0
G0/G1
S
G2/M
WT
TXNIP^KO
+ TXNIP
b
proliferation after exit from quiescence
fold increase confluency
3.5
3.0
2.5
2.0
1.5
1.0
0.5
WT
TXNIP^KO
SLC7A5^KO
TXNIP^KO SLC7A5^KO
0
12
24
36
48
time [h] growth after serum addition
c
continuous proliferation
fold increase in cell number
20
15
10
5
WT
TXNIP^KO
SLC7A5^KO
TXNIP^KO SLC7A5^KO
TXNIP^KO +TXNIP
TXNIP^KO +TXNIP^S308A
TXNIP^KO +TXNIP^S308D
0
24
48
72
time [h] - continuous growth
d
proliferating cell
quiescent cell
mTORC1
lysosome
AA
growth factors
AA
SLC3A2
SLC7A5
SLC1A5
AKT
P
S308
TXNIP
translation
mTORC1
lysosome
AA
AA
TXNIP
UB-ligase
Ub
Ub
AKT
lysosome
mTORC1

Figure 7

Figure 7. TXNIP mediated degradation of SLC7A5 contributed to the regulation of cell proliferation.

(a) WT, $TXNIP^{KO}$ and $TXNIP^{KO}$ cells reconstituted with TXNIP were harvested, permeabilized and fixed. The DNA content was analyzed by PI staining to assess the cell cycle profile by FACS (n=3, N>4000 cells). **(b)** Increase in confluency of the indicated cells, after refeeding serum starved cells, was measured by continuous live cell microcopy in an Incucyte incubator for 48 h (n=6). **(c)** The proliferation of the indicated cells was determined using CASY cell counting during the indicated time. The relative increase in cell number is normalized to 0 h and show as fold increase (n>3). **(d)** Model of TXNIP mediated downregulation of SLC7A5 during entry into quiescence.

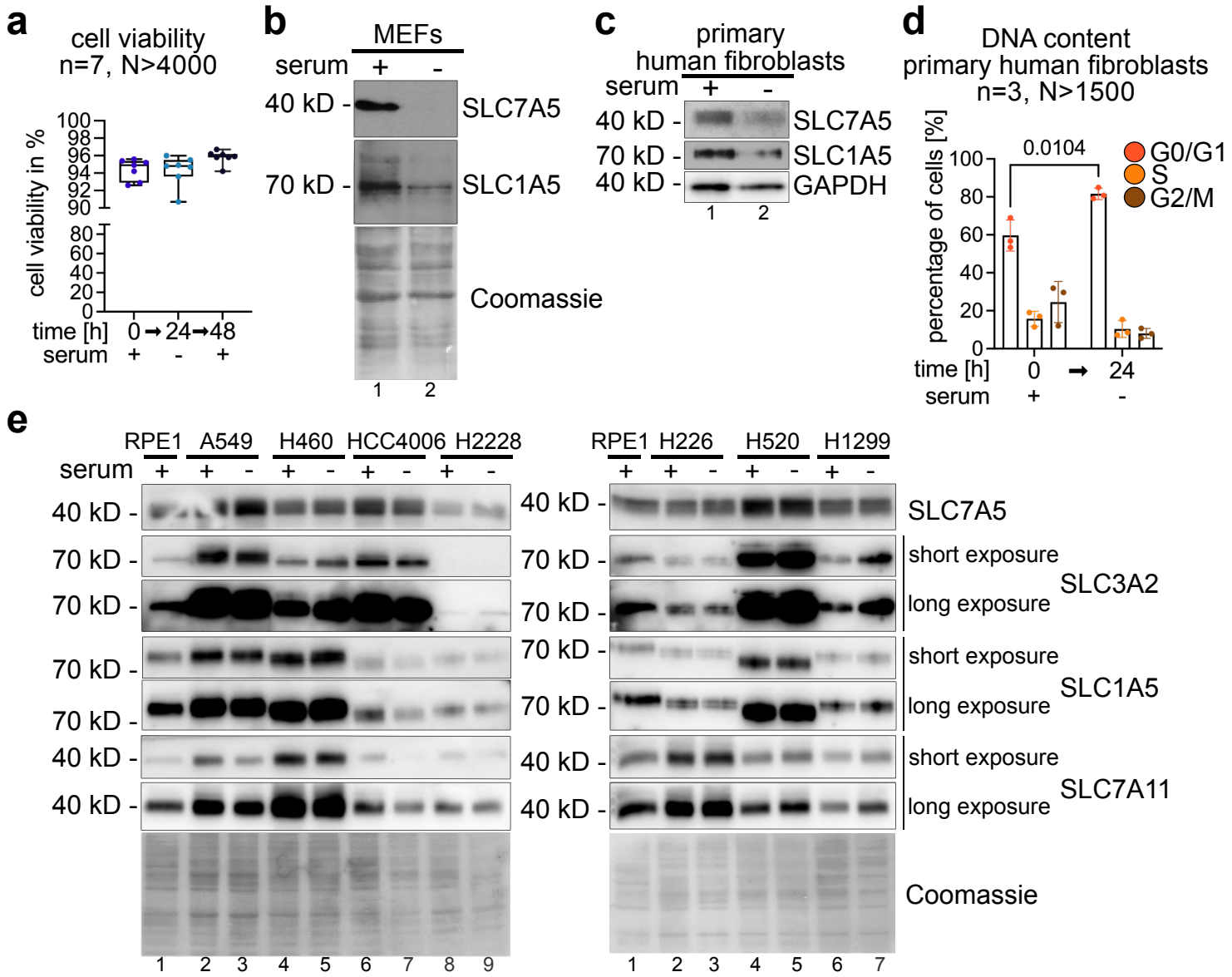

Supplementary Figure 1

Supplementary Figure 1. (a) Cell viability determined with CASY counter, before and after serum starvation and after re-addition of serum (n=7, N>4000 cells). **(b)** Immortalized MEFs were grown in growth medium with serum (+ serum) or serum starved for 24 h. Total cell lysates were analyzed by SDS-PAGE and WB with the indicated antibodies. **(c, d)** Primary human fibroblasts were grown in growth medium (+ serum) or serum starved for 24 h. **(c)** Total cell lysates were analyzed by SDS-PAGE and WB with the indicated antibodies. **(d)** Cells were harvested, permeabilized and fixed. The DNA content was analyzed by PI staining and FACS (n=3, N>1500 cells, two-way ANOVA, Tukey's multiple comparisons test). **(e)** Total cell lysates of the indicated cell lines were analyzed by SDS-PAGE and WB with the indicated antibodies. (**f, g)** Indirect IF of PFA fixed cells stained for **(f, g)** SLC1A5 (green), **(f)** LAMP1 (red) and DAPI (blue) were analyzed by confocal microscopy. The merged images show a single plane of a Z-stack. **(f)** Incubation with 12,5 µM chloroquine (CQ) in absence of serum for 14 h (- serum, + CQ). Scale bar=10 µm **(g)** Incubation with 20 µM dynasore (dyna) in absence of serum for 14 h (- serum, + dyna). Scale bar=10 µm. **(h)** Cells were incubated with [^{14}C]-glutamine for 15 min, washed and lysed. Total cell lysates were analyzed by scintillation counting. Cpm values were normalized to total protein content (cpm / µg protein, n=4, paired t-test).

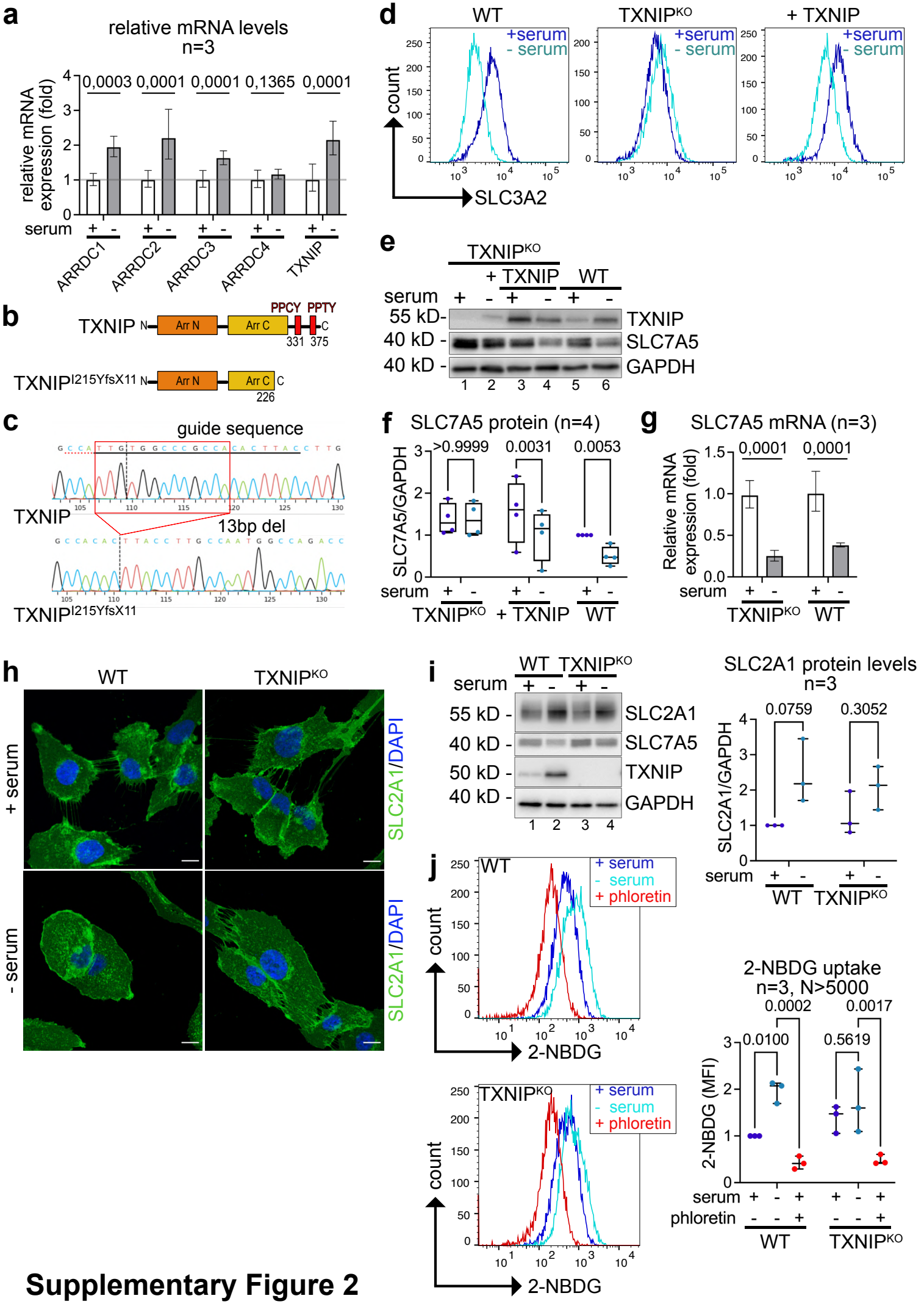

Supplementary Figure 2

Supplementary Figure 2. (a, g) qPCR analysis of **(a)** α-arrestins mRNA or **(g)** SLC7A5 mRNA in growing (+ serum) or serum starved cells (- serum). Expression levels were normalized to the housekeeping gene *RPLP0* (n=3, paired t-test). **(b)** Schematic presentation of the mutation introduced into TXNIP by gene editing. **(c)** Representative chromatogram of Sanger sequencing from the genome amplicon of WT TNIXP and gene edited TXNIP cells. The guide RNA and the protospacer adjacent motif (PAM) sequence are indicated. The vertical lane shows the Cas9 cleavage site causing a 13 base pair deletion in *TXNIP* (red box). Image was generated by the ICE Analysis online tool (Synthego, v2.0; Synthego, USA). **(d)** Representative histograms of SLC3A2 cell surface FACS from WT, $TXNIP^{KO}$ and $TXNIP^{KO}$ reconstituted with TXNIP cells. **(e)** WT, $TXNIP^{KO}$ and $TXNIP^{KO}$ reconstituted with TXNIP were grown in growth medium (+ serum) or serum starved for 24 h (- serum). Total cell lysates were analyzed by SDS-PAGE and WB with the indicated antibodies. **(f)** WB quantification of SLC7A5 protein levels, normalized to GAPDH (n=4, two-way ANOVA, Sidak's multiple comparisons test). **(h)** Indirect IF of PFA fixed WT and $TXNIP^{KO}$ cells stained for SLC2A1 (green) and DAPI (blue) was analyzed by confocal microscopy. The merged images show a single plane of a Z-stack. Scale bar=10 µm **(i)** Total cell lysates were analyzed by SDS-PAGE and WB with the indicated antibodies. For WB quantification, SLC2A1 protein levels were normalized to GAPDH (n=3, two-way ANOVA, Sidak's multiple comparisons test). **(j)** WT and $TXNIP^{KO}$ cells were assessed for glucose uptake by incorporation of 100 µM 2-NBDG for 45 min. Simultaneously, cells were treated with 1 mM phloretin. The fluorescence intensity was analyzed by FACS (n=3, N>5000 cells, two-way ANOVA, Sidak's multiple comparisons test).

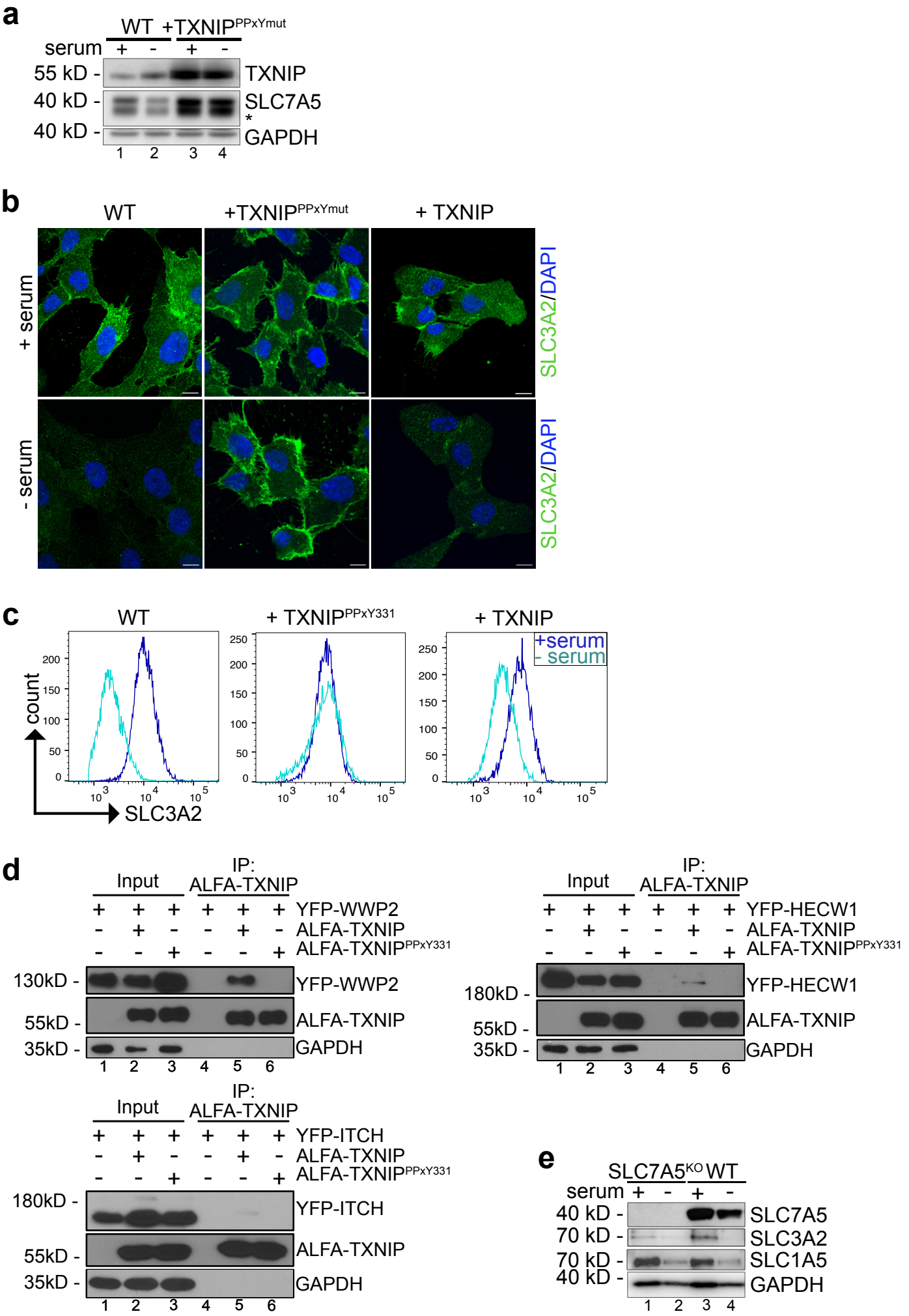

Supplementary Figure 3

Supplementary Figure 3. (a) Total cell lysates from WT or TXNIP^{KO} cells reconstituted with TXNIP^{PPxYmut} mutants were analyzed by SDS-PAGE and WB with the indicated antibodies. The asterisk (*) labels a second band that was only detected using the monoclonal SLC7A5 antibody. **(b)** Indirect IF of PFA fixed cells (WT, TXNIP^{KO} cells reconstituted with TXNIP or TXNIP^{PPxYmut}) stained for SLC3A2 (green) and DAPI (blue) was analyzed by confocal microscopy. The images show a single plane of a Z-stack. Scale bar = 10 µm. **(c)** Representative histograms of SLC3A2 cells surface FACS of the indicated cells. **(d)** SDS-PAGE and WB analysis with the indicated antibodies from non-denaturing ALFA-immunoprecipitations (IP) from HEK293T cells expressing ALFA-TXNIP or the mutated ALFA-TXNIP^{PPxY331} variant and the indicated YFP-tagged HECT-type ubiquitin ligase. **(e)** SDS-PAGE and WB with the indicated antibodies of SLC7A5^{KO} and WT cells.

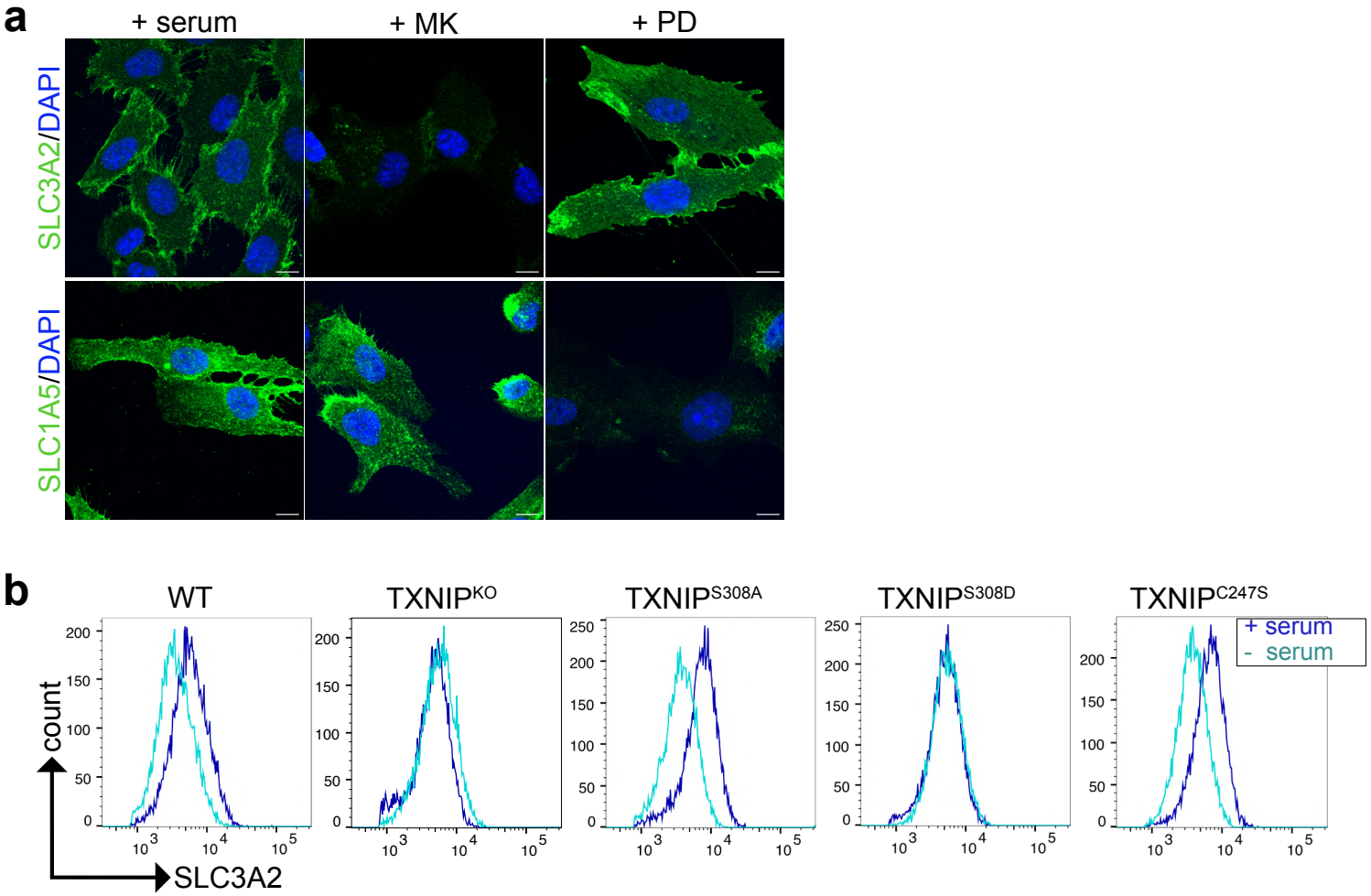

Supplementary Figure 4

Supplementary Figure 4. (a) Indirect IF of PFA fixed cells before or after serum starvation or incubation with 1 μM MK2206 (MK) or 5 μM PD0325901 (PD) stained for SLC3A2 (green, upper row) or SLC1A5 (green, lower row), and DAPI (blue). Cells were analyzed by confocal microscopy. The images show a single plane of a Z-stack. Scale bar = 10 μm. **(b)** Representative histograms of SLC3A2 cells surface FACS of the indicated cells.

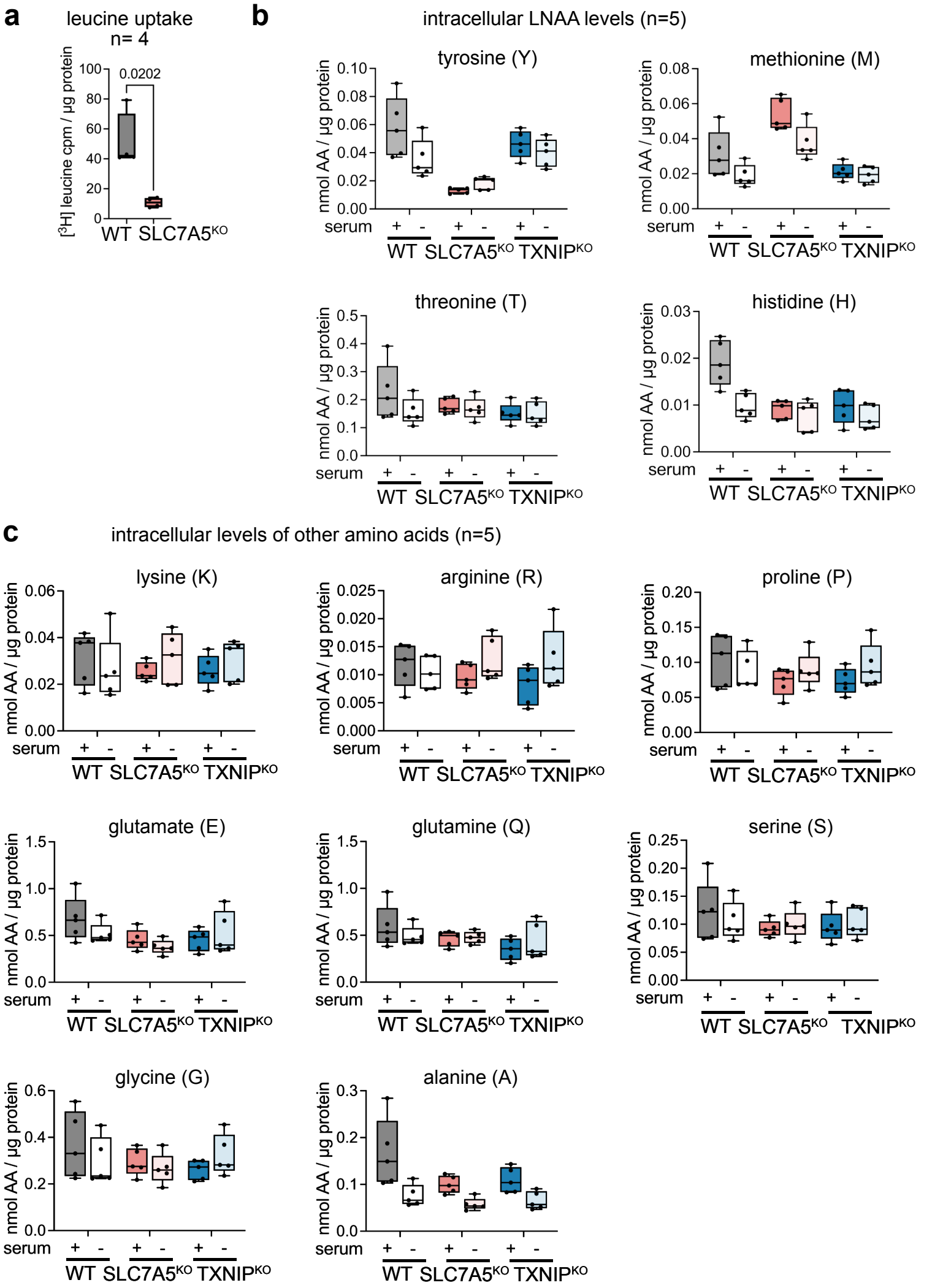

Supplementary Figure 5

Supplementary Figure 5. (a) WT and SLC7A5^{KO} cells were incubated with [^{3}H]-leucine for 15 min, washed and lysed. Cell lysates were analyzed by scintillation counting. Cpm values were normalized to total protein content (n=4, paired t-test). **(b, c)** WT, SLC7A5^{KO} and TXNIP^{KO} cells were grown in growth medium (+ serum) or serum starved for 24 h (- serum). Mass spectrometry analysis of free AAs, normalized to total protein content (nmol AA / µg protein, n=5).

Supplementary Table 1. AA, glucose and lactate levels in blood plasma of the TXNIP deficient patient over the indicated years.

AA [µmol/l]	**06/2014**	**07/2014**	**Reference values**	**02/2016**	**03/2018**	**11/2021**	**09/2022**	**Reference values**
leucine (L)	60.51	175.52	46 - 109	346.58	226.89	212.26	141.50	45 - 155
Isoleucine (I)	13.38	91.56	26 - 53	173.06	132.25	129.59	82.64	26 - 94
tryptophan (W)	25.21	51.44	n.a	76.35	45.51	40.21	41.48	n.a
valine (V)	99.97	148.00	57 - 262	529.46	376.67	389.20	229.86	57 - 270
phenylalanine (F)	46.45	41.50	23 - 110	84.41	54.64	53.02	56.75	23 - 70
methionine (M)	12.14	24.43	3 - 41	36.19	18.77	10.83	12.30	3 - 29
proline (P)	191.78	197.21	52 - 277	264.22	228.78	214.37	275.47	51 - 185
tyrosine (Y)	38.54	52.02	11 - 112	110.43	70.10	51.76	50.47	11 - 120
Fischer's ratio (FR)	2.05	4.46	2.10 - 4	5.38	5.90	6.98	4.23	2.10 - 4
glucose [mg/dl]	34	71	> 50	88 *	78	86	103	> 50
lactate [mg/dl]	68.30	46	5 - 22	24.33 *	50.5	26	56	5 - 22

* The glucose and lactate values were collected on a different day than the AA levels.

Supplementary Table 2. Summary of antibodies, reagents and software used in this study.

Reagents/resource	Reference or source	Identifier or catalog number	Additional information
Antibodies			
SLC1A5/ASCT2	Merck	#abn73, RRID:AB_10807715	WB (1:1000)
SLC1A5/ASCT2 (V501)	Cell Signaling	#5345, RRID:AB_10621427	WB (1:1000)
SLC1A5/ASCT2	Sigma-Aldrich	#HPA035240, RRID:AB_10604092	IF (1:50)
SLC7A5/LAT1 (polyclonal)	Cell Signaling	#5347S, RRID:AB_10695104	WB (1:2000)
SLC7A5/LAT1 (E9O4D) (monoclonal)	Cell Signaling	#32683	WB (1:2000)
SLC7A5/LAT1 (D10)	Santa Cruz	#sc-374232, RRID:AB_10988206	WB (1:100)
SLC3A2/4F2hc (D6O3P)	Cell Signaling	#13180S, RRID:AB_2687475	WB (1:1000)
SLC3A2/4F2hc	BD Biosciences	#556074, RRID:AB_396341	IF, FACS (1:100)
SLC2A1/Glut1	Merck	#07-1401, RRID:AB_1587074	WB (1:2000), IF (1:200)
SLC38A2/SNAT2	MBL International	#BMP081, RRID:AB_10597880	WB (1:100)
SLC7A11/xCT (D2M7A)	Cell Signaling	#12691, RRID:AB_2687474	WB (1:1000)
TXNIP (D5F3E)	Cell Signaling	#14715S, RRID:AB_2714178	WB (1:2000)
p-S6K^{T389} (108D2)	Cell Signaling	#9234S, RRID:AB_2269803	WB (1:1000)
S6K	Cell Signaling	#9202S, RRID:AB_331676	WB (1:1000)
p-S6$^{S240/244}$	Cell Signaling	#2215S, RRID:AB_331682	WB (1:2000)
S6 (54D2)	Cell Signaling	#2317S, RRID:AB_2238583	WB (1:1000)
p-ERK1/2$^{T202/Y204}$ (D13.14.4E)	Cell Signaling	#4370S, RRID:AB_2315112	WB (1:1000)
ERK1/2	Cell Signaling	#9102S, RRID:AB_330744	WB (1:1000)
p27^{Kip1} (D69C12)	Cell Signaling	#3686S, RRID:AB_2077850	WB (1:1000)
p-AKT^{S473} (D9E)	Cell Signaling	#4060S, RRID:AB_2315049	WB (1:1000)
p-AKT^{T308}	Cell Signaling	#9275, RRID:AB_329828	WB (1:1000)
AKT	Cell Signaling	#9272S, RRID:AB_329827	WB (1:1000)

ALFA	NanoTag Biotechnologies	#N1581, RRID:AB_3075997	WB (1:1000), IF (1:100)
Transferrin Receptor (Tfr)	DSHB	#G1/221/12, RRID:AB_2201506	WB (1:1000)
EGF Receptor (EGFR) (1005)	Santa Cruz	#sc-03-G	WB (1:500)
GAPDH (D4C6R)	Cell Signaling	#97166S, RRID:AB_2756824	WB (1:5000)
LAMP1	DSHB	#H4A3, RRID:AB_2296838	IF (1:50)
LAMP1 (D2D11)	Cell Signaling	#9091, RRID:AB_2687579	IF (1:800)
NEDD4	Cell Signaling	#5344S, RRID:AB_10560514	WB (1:1000)
WWP1	Cell Signaling	#70140S, RRID:AB_3662810	WB (1:1000)
WWP2	Cell Signaling	#41182S, RRID:AB_3662809	WB (1:1000)
ITCH	Cell Signaling	#12117S, RRID:AB_2797822	WB (1:1000)
GFP	Roche Life Science	(Roche Cat# 11814460001, RRID:AB_390913)	WB (1:1000)
Ubiquitin (P4D1)	Santa Cruz	#3936S, RRID:AB_628423	WB (1:500)
Goat anti-mouse IgG-peroxidase	Sigma-Aldrich	#A4416, RRID:AB_258167	WB (1:5000)
Goat anti-rabbit IgG-peroxidase	Sigma-Aldrich	#A0545, RRID:AB_257896	WB (1:5000)
Alexa Fluor 488 goat anti-rabbit IgG	Invitrogen	#A11008, RRID:AB_143165	IF (1:500)
Alexa Fluor 488 goat anti-mouse IgG	Invitrogen	#A11001, RRID:AB_2534069	IF (1:500)
Alexa Fluor 568 goat anti-mouse IgG	Invitrogen	#A11031, RRID:AB_144696	IF (1:500)
Alexa Fluor 568 goat anti-rabbit IgG	Invitrogen	#A11011, RRID:AB_143157	IF (1:500)
Chemicals			
Blasticidin	InvivoGen	#ant-bl-5b	
High glucose Dulbecco's modified Eagle's medium (DMEM)	Sigma-Aldrich	#D6429	
FSB	Sigma-Aldrich	#S0615	
Trypsin-EDTA solution	Sigma-Aldrich	#T4174	
MK2206	Enzo Life Sciences	#ENZ-CHM164-0005	
PD0325901	Absource	#S1036	
JPH203	Selleckchem,	#S8667	

chloroquine	Sigma-Aldrich	#C6628	
dynasore hydrate	Sigma-Aldrich	#D7693	
penicillin/streptomycin	Sigma-Aldrich	#P0781	
WesternBright Chemiluminescence substrate solution (Advansta)	Biozym	#541005X	
Lipofectamin LTX reagent	Thermo Scientific	#15338-100	
polyethylenimine (PEI)	Polyscience	#23966-100	
Polybrene	Sigma-Aldrich	#107689	
DAPI	Sigma-Aldrich	#D9542	
Mowiol	Sigma-Aldrich	#81381	
saponin	BioChemika	#84510	
RNAse A	Thermo Scientific	#EN0531	
[$^{14}C_5$]-L-glutamine	Hartmann Analytic	#MC1124	
[4,5-^{3}H]-L-Leucine	Hartmann Analytic	#MT672E	
[$^{14}C_5$]-L-Isoleucine	Hartmann Analytic	#MC174	
glutamine-free DMEM	Sigma-Aldrich	#D6546	
AA free DMEM	USBiological	#D9811-01	
2-NBDG	AAT Bioquest	#36702	
phloretin	Sigma-Aldrich	#P7912	
stable isotope-labeled canonical AA mix composition	Cambridge Isotope Laboratory	#MSK-CAA-1	
Cycloheximide	Sigma	Cat. # C7698	
anti-ALFA selector ST magnetic beads	NanoTag Biotechnologies	Cat. # N1516	
Critical commercial assays			
Micro BCA Protein Assay Kit	Thermo Scientific	#23235	
RNeasy Mini Kit	Quiagen	#74104	
LunaScript RT Super Mix Kit	NEB	#E3010	
Biozym Blue S'Green qPCR Kit	Biozym	#F-415S	
Software, algorithm			
Image J		Version 1.53t, RRID:SCR_003070	
Affinity Designer	Serfi	Version 1.10.5, RRID:SCR_016952	
GraphPad Prism 9		Version 9.4.1, RRID:SCR_002798	
Benchling		RRID:SCR_013955	
Flow Jo		Version 10.8.1, RRID:SCR_008520	
ModFit LT		RRRID:SCR_016106	

Primer3		Version 4.1.0, RRID:SCR_003139	
PrimerBank		RRID:SCR_006898	
CHOPCHOP		RRID:SCR_015723	
ZEISS ZEN Digital Imaging for Light Microscopy		Version 3.5, RRID:SCR_013672	
PrimerQuest™ Tool	Integrated DNA Technologies, IDT		
ICE Analysis online tool	Synthego, USA	Synthego, v2.0	

Supplementary Table 3: List of oligonucleotides used in this study

Name	**Vector backbone**	**Origin**
TXNIP	pCCL-EIF1α-BlastiR-DEST	This study
ALFA-TXNIP	pCCL-EIF1α-BlastiR-DEST	This study
SLC7A5-ALFA	pCCL-EIF1α-BlastiR-DEST	This study
TXNIP^{S308A}/ ALFA-TXNIP^{S308A}	pCCL-EIF1α-BlastiR-DEST	This study
TXNIP^{S308D}/ALFA-TXNIP^{S308D}	pCCL-EIF1α-BlastiR-DEST	This study
TXNIP$^{C247S/}$ALFA-TXNIP^{C247S}	pCCL-EIF1α-BlastiR-DEST	This study
ALFA-TXNIP p.Ile215TyrfsTer59	pCCL-EIF1α-BlastiR-DEST	This study
ALFA-TXNIP^{PPxY331AAxA,PPxY375AAxA}	pCCL-EIF1α-BlastiR-DEST	This study
ALFA-TXNIP^{PPCY331AACA}	pCCL-EIF1α-BlastiR-DEST	This study
pVSV-G		Clonetech, #631530
psPAX2		Gift from Stephan Geley
pDONR-ALFA-MCS		Generated by Michael Widerin
pDONR-MCS-ALFA		Generated by Michael Widerin
pDONR-221		Invitrogen, #12536017
pCCL-EIF1α-BlastiR-DEST		Gift from Stephan Geley
pSpCas9(BB)-2A-GFP (PX458)		Addgene, #48138
YFP-NEDD4	pCR3.1	[41], [42]
YFP-ITCH	pCR3.1	[41], [42]
YFP-WWP1	pCR3.1	[41], [42]
YFP-WWP2	pCR3.1	[41], [42]
YFP-HECW1	pCR3.1	[41], [42]

YFP-HECW2	pCR3.1	[41], [42]

Supplementary Table 4: Primers for PCR-based genetic modifications and cloning

Name	Forward primer	Reverse primer
ALFA-TXNIP	tAAgcagAAttcAatggtgatgttcAAgAAgatc	TGCTTAgtcgacTCACTGCACATTGTTGTTGA
attB-TXNIP	CAAAAAAGCAGGCTCCGCCACCATGGTGATGTTCAAGAAGATCAAGTC	CAAGAAAGCTGGGTCTCACTGCACATTGTTGTTGAGG
SLC7A5-ALFA	TAAGCAGTCGACatggcgggtgcgggcccg	TGCTTAGAATTCtgtctcctgggggaccac
Gateway	GGGGACAAGTTTGTACAAAAAAGCAGGCTCC	GGGGACCACTTTGTACAAGAAAGCTGGGTC
TXNIP^{S308A}	gcagAAcatccGCGatggccag	gttcggctggccatCGCggatgttctgc
TXNIP^{S308D}	gcagAAcatccGACatggccagccg	gttcggctggccatGTCggatgttctgctg
TXNIP^{C247S}	tattatctcagggacaAGCgcatcatggcgtggc	ccacgccatgatgcGCTtgtccctgagatAAtatgattgcc
TXNIP$^{p.Ile215TyrfsTer59}$	agctgccTattgtggcccgccacacttac	gtAAgtgtggcgggccacAAtAggcagct
TXNIP^{PPxY331AAxA}	ataccccagAAgctGCAGCAtgcGCAatggatgtcattcc	caggAAtgacatccatTGCgcaTGCTGCagcttctggggtatc
TXNIP^{PPxY375AAxA}	ttcAAgttcatgccaGCAGCAactGCAactgaggtggatccctgc	gcagggatccacctcagtTGCagtTGCTGCtggcatgAActtgAA
ALFA-TAG	caggggtattgacatccaccagat	atctggtggatgtcAAtacccctg

Supplementary Table 5: qPCR Primers used in this study

Gene	Forward primer	Reverse primer	Source
RPLP0	TGGTCATCCAGCAGGTG TTCGA	ACAGACACTGGCAAC ATTGC GG	[69]
SLC7A5	ATCGGGAAGGGTGATG TGTCCAAT	CAAAGAGGCCGCTGT ATAATGCCA	[57]
ARRDC1	TAGTGGAGGAGGGTTA CTTCAAC	TCTGGGATGCTGTTC AGGTTC	PrimerBank ID (65288282c1)
ARRDC2	GATTTTGCGTTCTGAGG CTG	GCTTTCACCTTGTCG AATAGC	IDT
ARRDC3	TCTTGCCTCCACCTCTTT ATTC	TCGGAACCCACATCA ACTTG	IDT
ARRDC4	GTTCCTCTCGTCTGATT GTTCC	ATTGGCGACCATGTG TCGAAT	PrimerBank ID (190886441c 3)
TXNIP	GAGTACCTGCGCTATGA AGAC	TTTGAAGGATGTTCC CAGAGG	IDT